Copy 204
RM A52I30

RESEARCH MEMORANDUM

COMPARISON BETWEEN PREDICTION AND EXPERIMENT FOR ALL-MOVABLE WING AND BODY COMBINATIONS AT SUPERSONIC SPEEDS - DRAG DUE TO LIFT AND LIFT-DRAG RATIO

By Elliott D. Katzen and William C. Pitts

Ames Aeronautical Laboratory
Moffett Field, Calif.

NATIONAL ADVISORY COMMITTEE FOR AERONAUTICS

WASHINGTON

December 5, 1952

NATIONAL ADVISORY COMMITTEE FOR AERONAUTICS

RESEARCH MEMORANDUM

COMPARISON BETWEEN PREDICTION AND EXPERIMENT FOR ALL-MOVABLE WING AND BODY COMBINATIONS AT SUPERSONIC SPEEDS - DRAG DUE TO LIFT AND LIFT-DRAG RATIO

By Elliott D. Katzen and William C. Pitts

SUMMARY

A method is presented for predicting the drag due to lift and the lift-drag ratio of all-movable wing and body combinations and all-movable wings in the presence of bodies at supersonic speeds. The method is used to calculate these factors for configurations for which experimental data are available. Comparison of the calculated and experimental data indicates that the method can be used to predict the drag due to lift and lift-drag ratio with sufficient accuracy for many design purposes. In general, the predicted drag-rise factors are lower than the experimental values and the predicted lift-drag ratios are correspondingly higher than the experimental values.

INTRODUCTION

This report is the second of two reports on the characteristics of all-movable wings combined with bodies. The first report, reference 1, treated lift, pitching moment, and hinge moment. It was shown in reference 1 that the lift of a number of all-movable wing and body combinations of various plan forms at supersonic speeds can be predicted with reasonable accuracy by means of a simple, generalized method. The purpose of the present report is to extend this method to the prediction of the drag characteristics and to determine the applicability of the method by comparison with available experimental results.

NOTATION

A	aspect ratio of exposed wing panels joined together
A_p	plan-form area of body, square inches
c	chord of wing at any spanwise position, inches
$\bar{c}$	mean aerodynamic chord $\left(\frac{\int_r^s c^2 dy}{\int_r^s c\, dy}\right)$, inches
c_{d_c}	cross-flow section drag coefficient of a circular cylinder
C_D	drag coefficient, omitting base drag $\left(\frac{D}{q_o S_W}\right)$
ΔC_D	increment in drag coefficient $\left(C_D - C_{D_{min}}\right)$
$C_{D_{min}}$	minimum drag coefficient
C_{D_o}	experimental minimum drag coefficient for $\alpha = 0$ and $\delta = 0$
C_L	lift coefficient $\left(\frac{L}{q_o S_W}\right)$
C_{L_α}	lift-curve slope for variable α and fixed δ $\left(\frac{\partial C_L}{\partial \alpha}\right)$, per radian
C_{L_δ}	lift-curve slope for variable δ and fixed α $\left(\frac{\partial C_L}{\partial \delta}\right)$, per radian
ΔC_L	increment in lift coefficient $\left(C_L - C_{L_{D=min}}\right)$
$\left(C_{L_\alpha}\right)_W$	lift-curve slope due to angle of attack of wing alone, per radian
$C_{L_{D=min}}$	lift coefficient for minimum drag

$C_{L_{opt}}$ lift coefficient for maximum lift-drag ratio

c_r chord at wing-fuselage juncture, inches

c_t chord at wing tip, inches

D drag force, omitting base drag, pounds

g gap between wing and body, inches

$k_{B(W)}$ $\left(\frac{L_{B(W)}}{L_W}\right)_{\text{angle}}$ for zero angle of attack and varying wing deflection

$k_{W(B)}$ $\left(\frac{L_{W(B)}}{L_W}\right)_{\text{angle}}$ for zero angle of attack and varying wing deflection

$K_{B(W)}$ $\left(\frac{L_{B(W)}}{L_W}\right)_{\text{attack}}$ for zero wing deflection angle and varying angle of attack

$K_{W(B)}$ $\left(\frac{L_{W(B)}}{L_W}\right)_{\text{attack}}$ for zero wing deflection angle and varying angle of attack

K_N $\frac{L_N}{L_W}$

l body length, inches

l_a body length between wing trailing edge and body base, inches

l_f body length between tip of nose and wing leading edge, inches

L lift force, pounds

m cotangent of leading-edge sweep angle

M_o free-stream Mach number

q_o free-stream dynamic pressure, pounds per square inch

r	body radius at the wing position, inches
R	resultant force, pounds
Re	Reynolds number based on wing mean aerodynamic chord
s	semispan of wing-body combination
S_W	area of exposed wing panels, square inches
V_o	free-stream velocity, inches per second
x,y	Cartesian coordinates
α	angle of attack of body, radians unless otherwise specified
β	$\sqrt{M_o^2-1}$
βA	effective aspect ratio
$(\beta A)^*$	critical effective aspect ratio
δ	wing deflection angle, radians unless otherwise specified
Λ	leading-edge sweep angle, degrees
λ	wing taper ratio $\left(\frac{c_t}{c_r}\right)$
η	correction for three-dimensional effects on body

Subscripts

B(W)	body in presence of wing
C	wing-body combination
N	body nose, that part of the body forward of the leading edge of the wing-body juncture
W	wing alone

W(B) wing in presence of body[1]

α α variable, δ constant

δ δ variable, α constant

Cα wing-body combination with α variable, δ constant (Other compound subscripts to be interpreted similarly to Cα.)

THEORETICAL CONSIDERATIONS

The drag force due to lift on an all-movable wing and body combination is determined by the lift or resultant forces on the components of the combination and the inclination of the resultant forces. It was shown in reference 1 that the lift coefficients of the components of the combinations in the linear range of angle of attack and wing deflection angle are given by the following equations:

$$C_{L_{W(B)}} = \left[K_{W(B)}\,\alpha + k_{W(B)}\delta\right]\left(C_{L_\alpha}\right)_W \tag{1}$$

$$C_{L_{B(W)}} = \left[K_{B(W)}\,\alpha + k_{B(W)}\delta\right]\left(C_{L_\alpha}\right)_W \tag{2}$$

$$C_{L_N} = K_N\,\alpha\left(C_{L_\alpha}\right)_W \tag{3}$$

with the lift coefficient of the combination given by

$$C_{L_C} = C_{L_{W(B)}} + C_{L_{B(W)}} + C_{L_N} \tag{4}$$

The wing-alone lift-curve slope, $\left(C_{L_\alpha}\right)_W$, can be obtained by linear-theory or preferably from experimental results, if available. Linear-theory results were used in the present report. The values of K_N were obtained by the slender-body formula

$$K_N = \frac{2\pi r^2}{S_W\left(C_{L_\alpha}\right)_W} \tag{5}$$

[1]In this report attention is focused on wings mounted on a section of uniform diameter.

Charts for determining the other parameters of equations (1) through (3), $K_{W(B)}$, $K_{B(W)}$, $k_{W(B)}$, and $k_{B(W)}$, are reproduced from reference 1 as figures 1, 2, and 3. Values of $K_{B(W)}$ are given in figures 1 and 2. Figure 1 is to be used for low aspect ratio cases, that is,

$$\beta A \leq (\beta A)^* = \frac{4}{(1+\lambda)\left(\frac{1}{m\beta} + 1\right)}$$

For high aspect ratios, $\beta A > (\beta A)^*$, $K_{B(W)}$ is given in figure 2.

There are several solutions available for determining $k_{W(B)}$, for example, slender-body theory (fig. 1) for slender wing-body combinations with triangular wings and an exact linear theory solution for combinations with rectangular wings (fig. 3). Figure 3 shows that there is some difference between the two predictions, the maximum difference being about 10 percent, but generally the difference is much less. The linear-theory values of $k_{W(B)}$ are to be used for rectangular wings of effective aspect ratio 2 or greater. For the range of βA between 2 and 0, no linear-theory results for $k_{W(B)}$ are available. However, as βA approaches zero the wing-body combination becomes more slender, until at $\beta A = 0$ slender-body theory is exact for the combination. On the basis of these considerations $k_{W(B)}$ as given by slender-body theory is to be used for all combinations with rectangular wings with $\beta A < 2$.

By use of reversibility theorems for combinations with cylindrical bodies, the following equation can be shown to be valid under the assumptions of slender-body theory:

$$k_{B(W)} = K_{W(B)} - k_{W(B)} \tag{6}$$

The values of $k_{B(W)}$ as given by equation (6) are included in figure 1.

Values of C_{L_α} and C_{L_δ} of many combinations of all-movable wings and bodies were predicted by the foregoing methods and compared with experimental results in reference 1. The accuracy of the predicted C_{L_α} was good in the linear range of angle of attack and wing deflection angle. The predicted C_{L_δ} tended to be higher than the experimental quantities. The geometric properties and lift characteristics for the combinations analyzed in reference 1 for which experimental drag data are available are presented in table I.

Drag Characteristics and Lift-Drag Ratio

In the present development, the drag due to lift of a combination or its components is determined with the assumptions that the resultant forces on the components are given by equations (1) through (3) and that the resultant forces have the following inclinations (fig. 4): The resultant force on the wing is inclined at an angle $\alpha + \delta$ (no leading-edge suction),[2] the resultant force on the body exclusive of the body nose is inclined rearward at an angle α, and the resultant force on the body nose acts at a rearward inclination of $\alpha/2$ from the vertical in accordance with slender-body theory. If it is assumed that the skin friction remains constant with α or δ, then for the combination

$$C_{D_C} = C_{D_o} + \left\{\left[K_{W(B)}\ \alpha + k_{W(B)}\delta\right]\ (\alpha+\delta) + \left[K_{B(W)}\alpha + k_{B(W)}\delta\right]\ \alpha + K_N\alpha^2/2\right\}\left(C_{L_\alpha}\right)_W \tag{7}$$

where C_{D_o} is the drag coefficient at $\alpha = 0^\circ$ and $\delta = 0^\circ$.

Typical drag curves for a combination (combination 10, table I) with α variable for constant deflection angles of 0°, 7°, and 14° are shown in figure 5. Theoretical drag curves calculated on the basis of equation (7), using experimental values of C_{D_o}, are also shown. It can be seen that for the higher values of δ the experimental values of the minimum drag are underestimated by a large percentage (42 percent for $\delta = 14^\circ$). A better prediction of minimum drag can be obtained by considering the body-alone force due to cross-flow separation as discussed in reference 2. This is an approximation because the force on the body of the wing-body combination is undoubtedly different from that on the body alone. The increment in drag coefficient of the body alone due to cross-flow separation as given in reference 2 is

$$(C_D)_{B,C.F.} = \frac{A_p}{S_W} c_{d_c}\ \eta\ |\alpha^3| \tag{8}$$

[2]Although linear-theory results indicate that leading-edge suction should be realized for wings with subsonic leading edges, experience has shown that theory and experiment are usually in better accord for wing-body combinations if leading-edge suction is omitted for the wings.

This increment is added to the combination drag coefficient given in equation (7) and the result is shown in figure 5. The improvement in the agreement between prediction and experiment for the minimum drag at the higher values of δ is evident. At points other than near the minimum drag, the theoretical curves for which the effect of cross flow is omitted are in closer agreement with experiment than the curves with the effect of cross flow included. This can be explained by the following factors: (1) Near the minimum drag point for large deflection angles, the lift is negative on the body and positive on the wing and the downwash field behind the wing tends to increase the cross-flow separation on the rear of the body; (2) over most of the range of α the lift on both the body and the wing is positive and the downwash behind the wing decreases the cross flow. Thus, including a cross-flow correction only in calculating the minimum drag point of the drag polar is a step in the right direction. The desirability of including the effect of cross flow in determining the minimum drag point, as is done in this report, will be shown in a subsequent correlation chart. The cross-flow correction is only important when the angle of attack of the body is large at the minimum drag point (i.e., for large values of δ).

If δ is constant and α is varied or if α is constant and δ is varied, the drag curve for a combination or a wing in the presence of a body is a parabola of the form (see fig. 6)

$$C_D = C_{D_{min}} + \frac{\Delta C_D}{\Delta C_L{}^2}\left(C_L - C_{L_{D=min}}\right)^2 \tag{9}$$

where $\Delta C_D/\Delta C_L{}^2$ is a constant called the drag-rise factor, which defines the variation of the drag with lift, that is,

$$\Delta C_D = C_D - C_{D_{min}}$$

$$\Delta C_L{}^2 = \left(C_L - C_{L_{D=min}}\right)^2$$

The lift-drag ratio is given by the equation

$$\frac{L}{D} = \frac{C_L}{C_{D_{min}} + (\Delta C_D/\Delta C_L{}^2)\left(C_L - C_{L_{D=min}}\right)^2} \tag{10}$$

The maximum lift-drag ratio is

$$\left(\frac{L}{D}\right)_{max} = \frac{C_{L_{opt}}}{C_{D_{min}} + (\Delta C_D/\Delta C_L{}^2)\left(C_{L_{opt}} - C_{L_{D=min}}\right)^2} \tag{11}$$

where $C_{L_{opt}}$, the lift coefficient for $(L/D)_{max}$, is given by

$$C_{L_{opt}} = \sqrt{\frac{C_{D_{min}}}{\Delta C_D/\Delta C_L{}^2} + C_{L_{D=min}}{}^2} \tag{12}$$

The problem of predicting the drag curves and lift-drag ratio is thus reduced to the determination of $C_{D_{min}}$, $C_{L_{D=min}}$, and $\Delta C_D/\Delta C_L{}^2$. These parameters are given below for wing-body combinations and wings in the presence of bodies both for a variation of angle of attack with constant wing deflection and for a variation of wing deflection with constant angle of attack.

Variation with angle of attack.- If δ is constant and α is varied for the combination, equation (7) with the cross-flow term of equation (8) added can be written

$$\left(C_{D_{min}}\right)_{C\alpha} = C_{D_o} + \left\{\left[K_{W(B)} + K_{B(W)} + K_N/2\right]\alpha_{D=min}{}^2 + 2K_{W(B)}\,\delta\alpha_{D=min} + k_{W(B)}\delta^2\right\}\left(C_{L_\alpha}\right)_W + \frac{A_p}{S_W}\,c_{d_c}\,\eta\,|\alpha_{D=min}{}^3| \tag{13}$$

where

$$\alpha_{D=min} = \frac{-\left[K_N+2K_{W(B)}+2K_{B(W)}\right]\left(C_{L_\alpha}\right)_W + \sqrt{\left[K_N+2K_{W(B)}+2K_{B(W)}\right]^2\left(C_{L_\alpha}\right)_W^2 + 24\frac{A_p}{S_W}c_{d_c}\ \eta\ K_{W(B)}\delta\left(C_{L_\alpha}\right)_W\ \frac{\delta}{|\delta|}}}{-6\left(A_p/S_W\right)\ c_{d_c}\ \eta\left(\frac{\delta}{|\delta|}\right)}$$

The lift coefficient for minimum drag of the combination is

$$\left(C_{L_{D=min}}\right)_{C\alpha} = \left\{\left[K_{W(B)}+K_{B(W)}+K_N\right]\alpha_{D=min}+K_{W(B)}\delta\right\}\left(C_{L_\alpha}\right)_W + \frac{A_p}{S_W}\,c_{d_c}\,\eta\frac{\alpha_{D=min}}{|\alpha_{D=min}|}\alpha_{D=min}^2 \qquad (14)$$

The minimum drag coefficient with the effect of cross flow omitted is

$$\left(C_{D_{min}}\right)_{C\alpha} = C_{D_o} + \left[k_{W(B)} - \frac{2K_{W(B)}^2}{2K_{W(B)}+2K_{B(W)}+K_N}\right]\delta^2\left(C_{L_\alpha}\right)_W \qquad (15)$$

The drag-rise factor, neglecting cross flow, for the combination is

$$\left(\frac{\Delta C_D}{\Delta C_L^2}\right)_{C\alpha} = \frac{2K_{W(B)}+2K_{B(W)}+K_N}{2\left[K_{W(B)}+K_{B(W)}+K_N\right]^2\left(C_{L_\alpha}\right)_W} \qquad (16)$$

For the wing in the presence of the body

$$\left(C_{D_{min}}\right)_{W(B)\alpha} = C_{D_o} - \frac{1}{4K_{W(B)}}\left[k_{W(B)}-K_{W(B)}\right]^2 \delta^2 \left(C_{L_\alpha}\right)_W \tag{17}$$

$$\left(C_{L_{D=min}}\right)_{W(B)\alpha} = -\frac{1}{2}\left[K_{W(B)} - k_{W(B)}\right] \delta \left(C_{L_\alpha}\right)_W \tag{18}$$

$$\left(\frac{\Delta C_D}{\Delta C_L{}^2}\right)_{W(B)\alpha} = \frac{1}{K_{W(B)}\left(C_{L_\alpha}\right)_W} = \frac{1}{\left(C_{L_\alpha}\right)_{W(B)}} \tag{19}$$

Variation with wing deflection.- If δ is varied and α is constant, the following expression can be obtained from equation (7):

$$\left(C_{D_{min}}\right)_{C\delta} = C_{D_o} + \left[K_{W(B)}+K_{B(W)}+K_N/2 - \frac{K_{W(B)}{}^2}{k_{W(B)}}\right]\alpha^2 \left(C_{L_\alpha}\right)_W + \frac{A_p}{S_W} c_{d_c} \eta \left|\alpha^3\right| \tag{20}$$

The lift coefficient for minimum drag of the combination becomes

$$\left(C_{L_{D=min}}\right)_{C\delta} = \left[K_{W(B)}+K_{B(W)}+K_N - \frac{K_{W(B)}{}^2}{k_{W(B)}}\right] \alpha \left(C_{L_\alpha}\right)_W + \frac{A_p}{S_W} c_{d_c} \eta \frac{\alpha}{|\alpha|} \alpha^2 \tag{21}$$

and the drag-rise factor, regardless of whether the effect of cross flow is included or not, can be obtained as

$$\left(\frac{\Delta C_D}{\Delta C_L{}^2}\right)_{C\delta} = \frac{k_{W(B)}}{K_{W(B)}{}^2\left(C_{L_\alpha}\right)_W} = \frac{\left(C_{L_\delta}\right)_{W(B)}}{\left(C_{L_\alpha}\right)_{W(B)}{}^2} \tag{22}$$

For the wing in the presence of the body,

$$\left(C_{D_{min}}\right)_{W(B)\delta} = C_{D_o} - \frac{1}{4k_{W(B)}}\left[K_{W(B)} - k_{W(B)}\right]^2 \alpha^2 \left(C_{L_\alpha}\right)_W \tag{23}$$

$$\left(C_{L_{D=min}}\right)_{W(B)\delta} = \frac{1}{2}\left[K_{W(B)} - k_{W(B)}\right]\alpha\left(C_{L_\alpha}\right)_W \tag{24}$$

$$\left(\frac{\Delta C_D}{\Delta C_L{}^2}\right)_{W(B)\delta} = \frac{1}{k_{W(B)}\left(C_{L_\alpha}\right)_W} = \frac{1}{\left(C_{L_\delta}\right)_{W(B)}} \tag{25}$$

Wing deflection for minimum drag at a given C_L.- The wing deflection for minimum drag at a given lift coefficient can be determined by solving the following system of simultaneous equations:

$$\left.\begin{aligned} \frac{\partial C_D}{\partial \alpha} + \lambda\frac{\partial C_L}{\partial \alpha} &= 0 \\ \frac{\partial C_D}{\partial \delta} + \lambda\frac{\partial C_L}{\partial \delta} &= 0 \\ \text{with the constraining condition} \\ C_L &= \left\{\left[K_{W(B)} + K_{B(W)} + K_N\right]\alpha + K_{W(B)}\,\delta\right\}\left(C_{L_\alpha}\right)_W \end{aligned}\right\} \tag{26}$$

where λ is a Lagrangian multiplier. If the effect of cross flow is neglected, the drag coefficient is given by equation (7) and the lift coefficient is given in equation (26). Solution of the system of equations (26) gives the wing deflection for minimum drag at a given lift coefficient as

$$\delta = \frac{K_{W(B)}K_N C_L \Big/ \left(C_{L_\alpha}\right)_W}{2K_{W(B)}{}^2\left[K_{W(B)}+K_{B(W)}+K_N\right] - 2k_{W(B)}\left[K_{W(B)}+K_{B(W)}+K_N\right]^2 + K_{W(B)}{}^2 K_N} \tag{27}$$

The angle of attack required to maintain the given lift coefficient is determined with the substitution of this value of δ in equations (26). The minimum drag at the given lift coefficient is determined with the substitution of the values of α and δ calculated by the above method in equation (7). The procedure outlined above was carried out for the combinations listed in table I. For most of the combinations, the wing

deflection required for minimum drag due to lift at lift coefficients above 0.25 was negative and so large as to be impractical because of the large angles of attack required. However, for some of the combinations the calculations indicated a small decrease in the drag due to lift for moderate negative wing deflections compared to that for zero deflection. Similar results were found in reference 3.

RESULTS AND DISCUSSION

The experimental drag characteristics and lift-drag ratios of a number of all-movable wing and body combinations (references 4 through 8) have been investigated and compared with characteristics predicted by the method discussed under Theoretical Considerations. The geometric and aerodynamic properties of the combinations are summarized in table I. Some of the experimental data available were not used in the present report because of large uncertainties in the data.

Drag Characteristics

Variation with angle of attack.- Theoretical values of $\left(C_{D_{min}}\right)_{C\alpha}$, $\left(C_{L_{D=min}}\right)_{C\alpha}$, and $(\Delta C_D/\Delta C_L{}^2)_{C\alpha}$ have been computed from equations (13), (14), and (16) for the wing-body combinations and constant wing deflection angles listed in table I. Experimental results are listed in the table together with the computed quantities and both are shown in figures 7, 8, and 9. Theoretical values of $\left(C_{D_{min}}\right)_{C\alpha}$ and $\left(C_{L_{D=min}}\right)_{C\alpha}$ with the effect of cross flow omitted for δ larger than 7° are also shown in figures 7 and 8. The degree of correlation is indicated by the distance from the line of perfect agreement. The better agreement between the experimental $\left(C_{D_{min}}\right)_{C\alpha}$ and the theoretical results with cross flow included is evident. The experimental $\left(C_{L_{D=min}}\right)_{C\alpha}$ scatter randomly about the theoretical value of approximately zero. The scatter is nearly ± 0.035 and is due largely to asymmetry of the experimental curves. Evidence of this is shown by the fact that the experimental $\left(C_{L_{D=min}}\right)_{C\alpha}$ for $\delta = 0$ is sometimes as large as 0.025, even though the configurations are symmetrical and the correct $\left(C_{L_{D=min}}\right)_{C\alpha}$ must be zero.

In figure 9, the average theoretical values of $(\Delta C_D/\Delta C_L^2)_{C\alpha}$, except for the points bounded by a dashed line, are approximately 7 percent less than the experimental values. The bounded points, for which the theoretical value of $(\Delta C_D/\Delta C_L^2)_{C\alpha}$ is as much as 37 percent less than the experimental value, correspond to combination 16 of table I. This configuration consists of a small rectangular tail at the back end of a long body. For this configuration it is quite likely that the transition point on the body moved forward with increasing angle of attack, as it often does for a body alone (see, for instance, reference 9). This would cause an increase in $(\Delta C_D/\Delta C_L^2)_{C\alpha}$ not predicted by the theory. This viscous effect would be reduced at full-scale Reynolds numbers. The general tendency for the theoretical $(\Delta C_D/\Delta C_L^2)_{C\alpha}$ to be lower than the experimental values is possibly due, to a lesser extent than for the bounded points of figure 9, to the transition point on the body moving forward of the leading edge of the wing-body juncture with increasing angle of attack. Also, the correlation would have been improved if the resultant force on the body nose had been assumed to be perpendicular to the body axis instead of inclined rearward at $\alpha/2$ from the vertical in accordance with slender-body theory.

A typical example of the fit between an experimental drag curve and a theoretical curve defined by the parameters $\left(C_{D_{min}}\right)_{C\alpha}$, $\left(C_{L_{D=min}}\right)_{C\alpha}$, and $(\Delta C_D/\Delta C_L^2)_{C\alpha}$ is shown in figure 10. The curves apply to combination 10 of table I. The agreement between the experimental and theoretical drag curves is considered fair in that the predicted curves are sufficiently accurate for many design purposes.

The drag data available for wings in the presence of bodies are shown in figures 11, 12, and 13 corresponding to combinations 17, 18, and 19 of table I. The agreement between theory and experiment for these wings is at least as good as the agreement for the wing-body combinations discussed above.

Variation with wing deflection.- Experimental and theoretical $\left(C_{D_{min}}\right)_{C\delta}$, $\left(C_{L_{D=min}}\right)_{C\delta}$, and $(\Delta C_D/\Delta C_L^2)_{C\delta}$ are recorded in table I and presented in the correlation plots of figures 7, 8, and 9. The theoretical parameters were calculated using equations (20), (21), and (22). Theoretical points with cross flow omitted for α larger than 7° are also included in figures 7 and 8. The improvement in correlation with cross flow included is evident for both $\left(C_{D_{min}}\right)_{C\delta}$ and $\left(C_{L_{D=min}}\right)_{C\delta}$. Although the theoretical $\left(C_{D_{min}}\right)_{C\delta}$, $\left(C_{L_{D=min}}\right)_{C\delta}$, and $(\Delta C_D/\Delta C_L^2)_{C\delta}$ are

in general lower than the experimental quantities and there is a good deal of scatter for $(\Delta C_D/\Delta C_L^2)_{C\delta}$, the agreement between theory and experiment is considered fair. The values of $\left(C_{D_{min}}\right)_{C\delta}$ and $(\Delta C_D/\Delta C_L^2)_{C\delta}$ are not greatly different from the values of $\left(C_{D_{min}}\right)_{C\alpha}$ and $(\Delta C_D/\Delta C_L^2)_{C\alpha}$. However, $\left(C_{L_{D=min}}\right)_{C\delta}$ is always positive for positive α and greater than $\left(C_{L_{D=min}}\right)_{C\alpha}$. Also, the variation of $\left(C_{L_{D=min}}\right)_{C\delta}$ with α is much greater than the variation of $\left(C_{L_{D=min}}\right)_{C\alpha}$ with δ.

A typical example of the experimental drag curves and the theoretical curves defined by the parameters $\left(C_{D_{min}}\right)_{C\delta}$, $\left(C_{L_{D=min}}\right)_{C\delta}$, and $(\Delta C_D/\Delta C_L^2)_{C\delta}$ is shown in figure 10. Comparison of the data indicates that the drag characteristics of all-movable wing and body combinations can be predicted with fair accuracy by the method of the present report for varying wing deflection as well as for varying angle of attack.

Experimental and theoretical drag curves for wings in the presence of bodies are shown in figures 11, 12, and 13. The agreement between the theoretical and experimental curves is as good as that for the wing-body combinations.

Lift-Drag Ratio

Variation with angle of attack.- Theoretical and experimental lift-drag ratios for the wing-body combinations are presented as a function of lift coefficient for constant wing deflection in figure 14. In calculating the theoretical $(L/D)_{C\alpha}$, cross flow was used for $\left(C_{D_{min}}\right)_{C\alpha}$ and $\left(C_{L_{D=min}}\right)_{C\alpha}$ and neglected for $(\Delta C_D/\Delta C_L^2)_{C\alpha}$. The theoretical values of $(L/D)_{C\alpha}$ decreased slightly with increasing δ. This occurs experimentally for δ larger than 4° but for $\delta = 4^\circ$ the experimental $(L/D)_{C\alpha}$ are often (figs. 14(i), 14(j), and 14(k)) somewhat larger than for $\delta = 0$. In general, the theoretical and experimental curves are in good agreement for small δ but for $\delta = 14^\circ$ the theoretical values of $(L/D)_{C\alpha}$ for some configurations are as much as 25 percent higher than the experimental values.

Theoretical and experimental $(L/D)_{C\alpha}$ for combination 6, the only combination for which negative deflection data are available for $C_L > C_{L_{opt}}$, are shown in figure 14(p) for $\delta = 0$ and $\delta = -5^\circ$. This figure shows a significant increase in $(L/D)_{C\alpha}$ experimentally for $C_L > C_{L_{opt}}$ with $\delta = -5^\circ$ relative to that for $\delta = 0$. Although the theory should not be expected to be strictly applicable at large lift coefficients it can be expected to indicate trends. The theoretical increase in $(L/D)_{C\alpha}$ for negative deflection is somewhat less than that obtained experimentally. At $C_L = 0.95$ the predicted $(L/D)_{C\alpha}$ for $\delta = -5^\circ$ is 2 percent higher than for $\delta = 0$ and experimentally the increase is 8 percent.

Theoretical $(L/D)_{max_{C\alpha}}$ and $\left(C_{L_{opt}}\right)_{C\alpha}$ were calculated on the basis of equations (11), (12), (13), (14), and (16) and are presented together with experimental quantities in the correlation plots of figures 15 and 16. The theoretical $(L/D)_{max_{C\alpha}}$ averages approximately 10 percent higher than the experimental $(L/D)_{max_{C\alpha}}$ corresponding to the theoretical $\left(C_{D_{min}}\right)_{C\alpha}$ and $(\Delta C_D/\Delta C_L{}^2)_{C\alpha}$ tending to be lower than the experimental values. The line of best fit for the $\left(C_{L_{opt}}\right)_{C\alpha}$ correlation points coincides with the line of perfect agreement.

Variation with wing deflection.- Experimental and theoretical lift-drag ratios as a function of lift coefficient with wing deflection variable are shown in figure 17. The curves are presented for the wing-body combinations of table I for which sufficient experimental data were available for the necessary cross plots. The experimental and theoretical curves are in qualitative agreement in that the $(L/D)_{C\delta}$ for C_L greater than about 0.25 increase with increasing α. Also, C_L for maximum lift-drag ratio increases with increasing α. Quantitatively, the theoretical $(L/D)_{C\delta}$ averages approximately 10 percent higher than the experimental values over the complete range of C_L.

Experimental and theoretical $(L/D)_{max_{C\delta}}$ and $\left(C_{L_{opt}}\right)_{C\delta}$ are presented in the correlation plots of figures 15 and 16. The average theoretical $(L/D)_{max_{C\delta}}$ are approximately 9 percent higher than the experimental values and the average theoretical $\left(C_{L_{opt}}\right)_{C\delta}$ are approximately 3 percent higher than the experimental values.

CONCLUSIONS

A method has been presented for predicting the drag due to lift and the lift-drag ratio of all-movable wing and body combinations and all-movable wings in the presence of bodies at supersonic speeds. The method has been used to calculate these factors for configurations for which experimental data were available. Comparison of the calculated and experimental data affords the following conclusions:

1. The theoretical method presented can be used to predict the drag due to lift and lift-drag ratio with sufficient accuracy for many design purposes.

2. Generally, the predicted drag-rise factors were lower than the experimental values and the predicted lift-drag ratios were correspondingly higher than the experimental values.

3. The theoretical results indicated that for some wing-body combinations a small improvement in lift-drag ratio could be obtained with negative wing deflections. This was substantiated experimentally for the wing-body combination for which experimental data were available.

Ames Aeronautical Laboratory
National Advisory Committee for Aeronautics
Moffett Field, Calif.

REFERENCES

1. Nielsen, Jack N., Kaattari, George E., and Drake, William C.: Comparison Between Prediction and Experiment for All-Movable Wing and Body Combinations at Supersonic Speeds - Lift, Pitching Moment, and Hinge Moment. NACA RM A52D29, 1952.

2. Allen, H. Julian: Estimation of the Forces and Moments Acting on Inclined Bodies of Revolution of High Fineness Ratio. NACA RM A9I26, 1949.

3. Tucker, Warren A.: A Method for Estimating the Components of Lift of Wing-Body Combinations at Supersonic Speeds. NACA RM L52D22, 1952.

4. Peters, R. G.: Data Report for Supersonic Wind Tunnel Tests on GAPA Model FR-87, Fifth Aberdeen Test Period, M = 1.72. Boeing Aircraft Company, D-8397, (Tech. Rept. No. 111-7). Aug. 1947.

5. Peters, R. G.: Data Report for Supersonic Wind Tunnel Tests on GAPA Model FR-87, Sixth and Seventh Aberdeen Test Periods, M = 1.72 and M = 1.28. Boeing Aircraft Company, D-8788, (Tech. Rept. No. 111-9). Feb. 1948.

6. Ellis, Macon C., Jr., and Grigsby, Carl E.: Aerodynamic Investigation at Mach Number 1.92 of a Rectangular Wing and Tail and Body Configuration and Its Components. NACA RM L9L28a, 1950.

7. Delameter, H. D., Stamper, J. C., and Solvason, J. C.: Model XAAM-N-2. Preliminary Analysis of Force and Moment Characteristics from Supersonic Wind Tunnel Tests of a 45-Percent-Scale Semi-Span Model. Ballistic Research Lab., Aberdeen Proving Ground, Maryland, Mach No. = 1.72. Douglas Aircraft Co., Inc., SM 13469, Oct. 1949.

8. Conner, D. William: Aerodynamic Characteristics of Two All-Movable Wings Tested in the Presence of a Fuselage at a Mach Number of 1.9. NACA RM L8H04, 1948.

9. Katzen, Elliott D., and Kaattari, George E.: Drag Interference Between a Pointed Cylindrical Body and Triangular Wings of Various Aspect Ratios at Mach Numbers of 1.50 and 2.02. NACA RM A51C27, 1951.

TABLE I.– SUMMARY OF AERODYNAMIC AND GEOMETRIC CHARACTERISTICS AND TEST CONDITIONS FOR ALL-MOVABLE WING AND BODY COMBINATIONS

No.	Sketch	M_o	Re	Wing section	δ (in.)	$\frac{g}{\delta}$ (in.)	βM	λ	$\Lambda_{L.E.}$	$\frac{r}{s}$	r (in.)	l (in.)	l_a (in.)	l_f (in.)	$\left(\frac{A_p}{B_w}\right)_\eta$	Refer-ence	Facility
1		1.72	1.05×10^6	[1]hex.	2.49	- - -	1.87	0.130	60	0.265	0.50	12.00	2.04	6.26	1.23	4	Aberdeen
2		1.72	$.80\times10^6$	hex	1.90	- - -	2.80	.253	50	.228	.50	12.00	5.61	3.68	1.23	4	Aberdeen
3		1.28	1.05×10^6	hex	2.49	- - -	1.07	.130	60	.265	.50	12.00	4.97	3.35	1.23	5	Aberdeen
4		1.28	$.80\times10^6$	hex	1.90	- - -	1.60	.253	50	.228	.50	12.00	5.61	3.68	1.23	5	Aberdeen
5		2.07	$.64\times10^6$	[2]d.w.	1.50	0.005	7.25	0	45	.200	.56	10.5	4.50	3.75	1.42	-	Ames 1 × 3
6		1.46	$.81\times10^6$	d.w.	1.50	.005	4.26	0	45	.200	.56	10.5	4.50	3.75	1.42	-	Ames 1 × 3
7		1.15	1.25×10^6	d.w.	7.5%	.016	1.31	0	60	.216	1.80	57.31	25.08	20.92	1.75	-	Ames 6 × 6
8		1.20	1.25×10^6	d.w.	7.5%	.016	1.53	0	60	.216	1.80	57.31	25.08	20.92	1.75	-	Ames 6 × 6
9		1.30	1.25×10^6	d.w.	7.5%	.016	1.92	0	60	.216	1.80	57.31	25.08	20.92	1.75	-	Ames 6 × 6
10		1.40	1.25×10^6	d.w.	7.5%	.016	2.27	0	60	.216	1.80	57.31	25.08	20.92	1.75	-	Ames 6 × 6
11		1.53	1.25×10^6	d.w.	7.5%	.016	2.68	0	60	.216	1.80	57.31	25.08	20.92	1.75	-	Ames 6 × 6
12		1.70	1.25×10^6	d.w.	7.5%	.016	3.18	0	60	.216	1.80	57.31	25.08	20.92	1.75	-	Ames 6 × 6
13		1.40	1.25×10^6	d.w.	7.5%	.016	2.27	0	0	.216	1.80	57.31	25.08	23.63	1.75	-	Ames 6 × 6
14		1.40	1.51×10^6	d.w.	11.31	.016	1.13	1	0	.216	1.80	57.31	23.72	22.28	.87	-	Ames 6 × 6
15		1.90	1.51×10^6	d.w.	11.31	.016	1.87	1	0	.216	1.80	57.31	23.72	22.28	.87	-	Ames 6 × 6
16		1.92	$.2\times10^6$	[3]b.c.	0.62	.000	5.13	1	0	.228	.35	8.75	.08	8.05	3.06	6	Langley 9"x12"
17		1.72	3.92×10^6	d.w.	7.5%	- - -	3.24	0	60	.216	1.80	29.00	5.14	12.55	- - -	7	Aberdeen
18		1.90	1.9×10^6	b.c.	2.64	.005	3.74	0	60	.269	.80	19.20	5.63	9.61	- - -	8	Langley 9"x12"
19	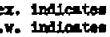	1.90	1.4×10^6	d.w.	1.87	.005	5.69	0	0	.232	.80	19.20	6.27	10.81	- - -	8	Langley 9"x12"

[1]hex. indicates hexagonal
[2]d.w. indicates double wedge
[3]b.c. indicates biconvex

TABLE I.- CONTINUED

No.	$\beta A(1+\lambda)\left(\frac{1}{m\beta}+1\right)$	K_W	$K_{B(W)}$	$K_{W(B)}$	$k_{W(B)}$	$k_{B(W)}$	C_{D_0}	Lift[1] $\beta(C_{L_\alpha})_W$	$\beta(C_{L_\alpha})_N$	$\beta(C_{L_\alpha})_{W(B)}$	$\beta(C_{L_\alpha})_C$	$\beta(C_{L_\delta})_{W(B)}$	$\beta(C_{L_\delta})_C$
1	4.7	0.12	0.33	1.22	0.938	0.28	0.033	--- (3.06)	0.44 (.38)	--- (3.74)	4.80 (6.12)	--- (2.87)	3.05 (3.74)
2	6.5	.20	.29	1.19	.941	.25	.038	--- (3.68)	.44 (.38)	--- (4.38)	5.36 (5.61)	--- (3.46)	3.49 (4.38)
3	3.8	.11	.39	1.22	.938	.28	.038	--- (2.04)	.47 (.22)	--- (2.49)	3.53 (3.51)	--- (1.91)	2.18 (2.49)
4	5.0	.08	.26	1.19	.961	.25	.039	--- (2.64)	.47 (.29)	--- (3.14)	4.03 (4.05)	--- (2.48)	2.74 (3.14)
5	11.2	.28	.23	1.16	.944	.28	.029	--- (4.00)	--- (.72)	--- (4.65)	7.31 (6.86)	--- (3.89)	4.87 (4.65)
6	8.24	.30	.22	1.16	.944	.22	.068						
7	5.5	.09	.27	1.18	.942	.24	.035	--- (1.86)	--- (.16)	--- (2.20)	3.01 (2.84)	--- (1.75)	--- (2.20)
8	5.5	.09	.26	1.18	.942	.24	.037	--- (2.11)	--- (.18)	2.57 (2.49)	3.39 (3.22)	--- (1.99)	--- (2.49)
9	5.91	.09	.25	1.18	.942	.24	.035	--- (2.31)	--- (.23)	3.09 (2.96)	3.95 (3.83)	--- (2.37)	--- (2.96)
10	6.3	.10	.25	1.18	.942	.24	.037	--- (2.63)	--- (.27)	3.54 (3.34)	4.41 (4.31)	2.47 (2.67)	2.81 (3.34)
11	6.7	.10	.25	1.18	.942	.24	.034	--- (3.17)	--- (.30)	3.85 (3.74)	4.88 (4.84)	--- (2.99)	3.09 (3.74)

Drag due to lift and lift-drag ratio[1] — Wing-body combinations

No.	α varying: δ°	$\left(\frac{\Delta C_D}{\beta C_L^2}\right)_\alpha$	$(C_{D_{min}})_\alpha$	$(C_{L_{D\text{-}min}})_\alpha$	$(C_{L_{opt}})_\alpha$	$\left(\frac{L}{D}\right)_{max_\alpha}$	δ varying: α°	$\left(\frac{\Delta C_D}{\Delta C_L^2}\right)_\delta$	$(C_{D_{min}})_\delta$	$(C_{L_{D\text{-}min}})_\delta$	$(C_{L_{opt}})_\delta$	$\left(\frac{L}{D}\right)_{max_\delta}$
1	0	0.25 (.26)	0.033 (.033)	0.00 (.00)	0.36 (.36)	5.00 (5.57)	0	0.34 (.29)	0.033 (.033)	0.00 (.00)	0.32 (.34)	4.57 (5.13)
	6	--- (.26)	--- (.034)	--- (-.01)	.35 (.36)	4.90 (5.19)	1.7	.33 (.29)	.035 (.035)	.02 (.01)	.31 (.34)	4.69 (5.23)
	10	--- (.26)	--- (.037)	--- (-.01)	.37 (.37)	4.51 (4.99)	--	---	---	---	---	---
2	0	.24 (.24)	.035 (.035)	.00 (.00)	.39 (.40)	4.98 (5.21)	0	.33 (.25)	.038 (.038)	.00 (.00)	.35 (.39)	4.39 (5.30)
	3	.26 (.24)	.039 (.038)	.00 (.00)	.38 (.40)	4.79 (5.16)	3	.32 (.25)	.040 (.038)	.03 (.01)	.35 (.39)	4.72 (5.29)
	6	.26 (.24)	.041 (.039)	-.02 (-.01)	.40 (.40)	4.62 (5.13)	6	.30 (.25)	.047 (.039)	.06 (.02)	.39 (.39)	5.07 (5.33)
	10	.27 (.24)	.048 (.040)	-.02 (-.01)	.42 (.41)	4.29 (5.03)	10	--- (.25)	--- (.043)	--- (.05)	.43 (.42)	5.06 (5.43)
3	0	.30 (.22)	.038 (.038)	.00 (.00)	.41 (.41)	5.50 (5.46)	--	---	---	---	---	---
	6	.23 (.23)	.042 (.040)	.08 (-.02)	.43 (.43)	5.31 (5.25)	--	---	---	---	---	---
4	0	.18 (.19)	.039 (.039)	.01 (.00)	.46 (.49)	5.66 (5.76)	0	.23 (.20)	.039 (.039)	.00 (.00)	.38 (.44)	5.09 (5.64)
	6	.19 (.19)	.044 (.040)	-.02 (-.02)	.52 (.49)	5.44 (5.68)	--	---	---	---	---	---
	10	.20 (.19)	.050 (.042)	-.01 (-.01)	.52 (.47)	4.99 (5.29)	--	---	---	---	---	---
5	0	.27 (.27)	.055 (.055)	.00 (.00)	.48 (.49)	4.08 (4.09)	0	.35 (.38)	.055 (.055)	.00 (.00)	.38 (.48)	3.54 (3.75)
	2.34	.27 (.27)	.057 (.055)	.00 (.00)	.46 (.45)	4.09 (4.03)	2	.34 (.38)	.055 (.055)	.02 (.01)	.39 (.48)	3.76 (3.90)
	3.08	.26 (.27)	.056 (.055)	.00 (-.01)	.43 (.45)	4.06 (4.02)	4	.33 (.38)	.056 (.056)	.03 (.03)	.41 (.48)	3.98 (4.05)
	4.76	.26 (.27)	.057 (.056)	.00 (-.01)	.44 (.49)	4.08 (3.97)	6	.35 (.38)	.065 (.058)	.06 (.05)	.44 (.48)	4.00 (4.15)
	8.11	.31 (.27)	.060 (.059)	.00 (-.01)	.48 (.47)	3.72 (3.87)	--	---	---	---	---	---
	12.18	--- (.27)	--- (.065)	--- (-.01)	.45 (.49)	3.44 (3.68)	--	---	---	---	---	---
6	0	.18 (.18)	.068 (.066)	.00 (.00)	.55 (.61)	4.16 (4.46)	--	---	---	---	---	---
	-5	.18 (.18)	.072 (.069)	.01 (.01)	.56 (.61)	4.88 (4.53)	--	---	---	---	---	---
7	0	.22 (.19)	.035 (.035)	-.01 (.00)	.40 (.43)	5.38 (6.10)	--	---	---	---	---	---
8	0	.22 (.20)	.037 (.037)	.00 (.00)	.48 (.43)	5.54 (5.99)	--	---	---	---	---	---
9	0	.24 (.21)	.035 (.035)	.00 (.00)	.37 (.41)	5.40 (5.82)						
10	0	.27 (.22)	.035 (.035)	.00 (.00)	.39 (.40)	5.05 (5.71)	0	.30 (.23)	.035 (.035)	.00 (.00)	.33 (.39)	4.93 (5.72)
	4	.24 (.22)	.037 (.035)	.01 (.00)	.40 (.40)	5.45 (5.68)	4	.30 (.23)	.039 (.036)	.06 (.02)	.38 (.39)	5.53 (5.77)
	7	.23 (.22)	.043 (.037)	.00 (.00)	.41 (.41)	4.96 (5.52)	7	.30 (.23)	.046 (.039)	.09 (.05)	.42 (.41)	5.48 (5.92)
	10	.22 (.22)	.049 (.040)	.00 (.00)	.48 (.43)	4.59 (5.33)	10	.31 (.23)	.056 (.046)	.14 (.09)	.45 (.45)	5.28 (5.07)
	14	.23 (.22)	.060 (.048)	--- (.01)	.45 (.47)	3.80 (4.94)	—		—			
11	0	.25 (.23)	.034 (.034)	.00 (.00)	.38 (.38)	5.15 (5.64)	0	.32 (.25)	.034 (.034)	.00 (.00)	.35 (.37)	4.65 (5.49)
	4	.25 (.23)	.034 (.034)	.00 (.00)	.38 (.38)	5.40 (5.56)	4	.32 (.25)	.035 (.035)	.04 (.02)	.35 (.37)	5.34 (5.70)
	7	.24 (.23)	.040 (.036)	-.02 (.00)	.37 (.39)	4.85 (5.45)	7	.31 (.25)	.042 (.038)	.08 (.05)	.39 (.39)	5.38 (5.85)
	10	.24 (.23)	.043 (.039)	-.03 (.00)	.37 (.41)	4.41 (5.29)	10	.30 (.25)	.052 (.045)	.16 (.08)	.44 (.44)	5.28 (5.80)
	14	.24 (.23)	.048 (.047)	.00 (.01)	.43 (.45)	3.63 (4.88)		---	---	---	---	---

[1]In each case the experimental value is given first and the corresponding theoretical value indicated in parenthesis directly below.

NACA

TABLE I.- CONCLUDED

[redacted]

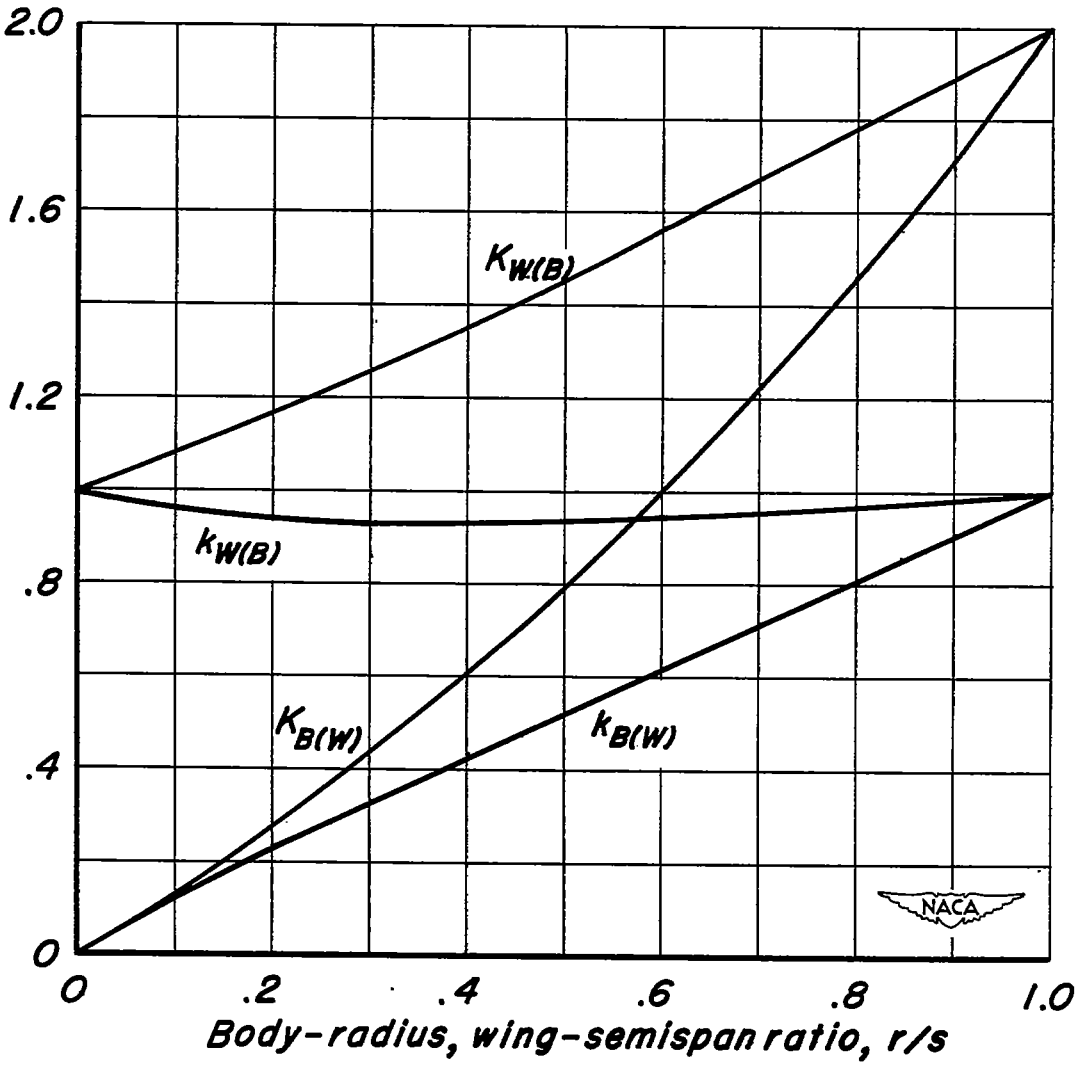

Figure 1.- Values of $K_{W(B)}$, $K_{B(W)}$, $k_{W(B)}$, and $k_{B(W)}$ from slender-body theory.

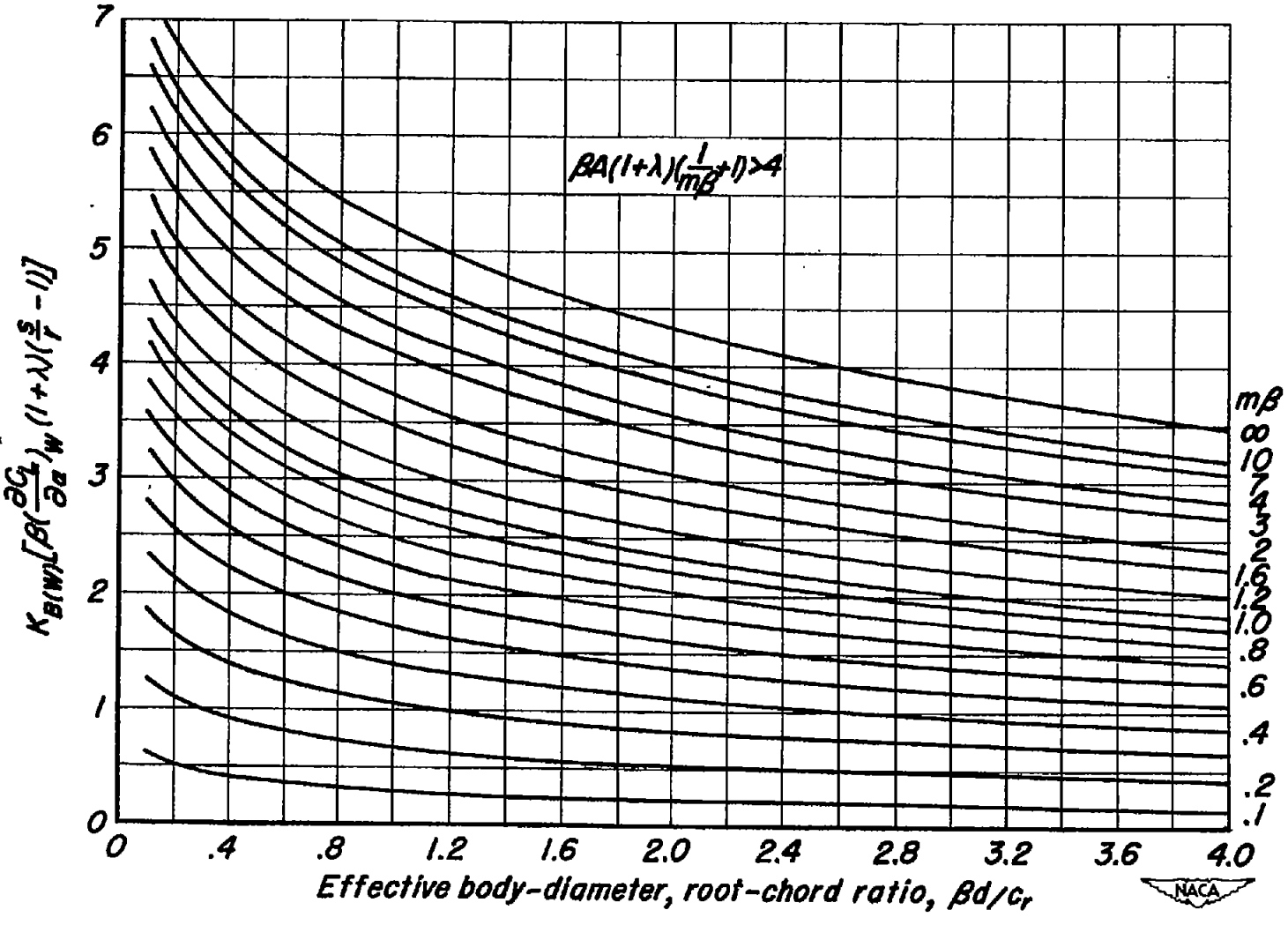

Figure 2.- Design chart for determination of $K_{B(W)}$.

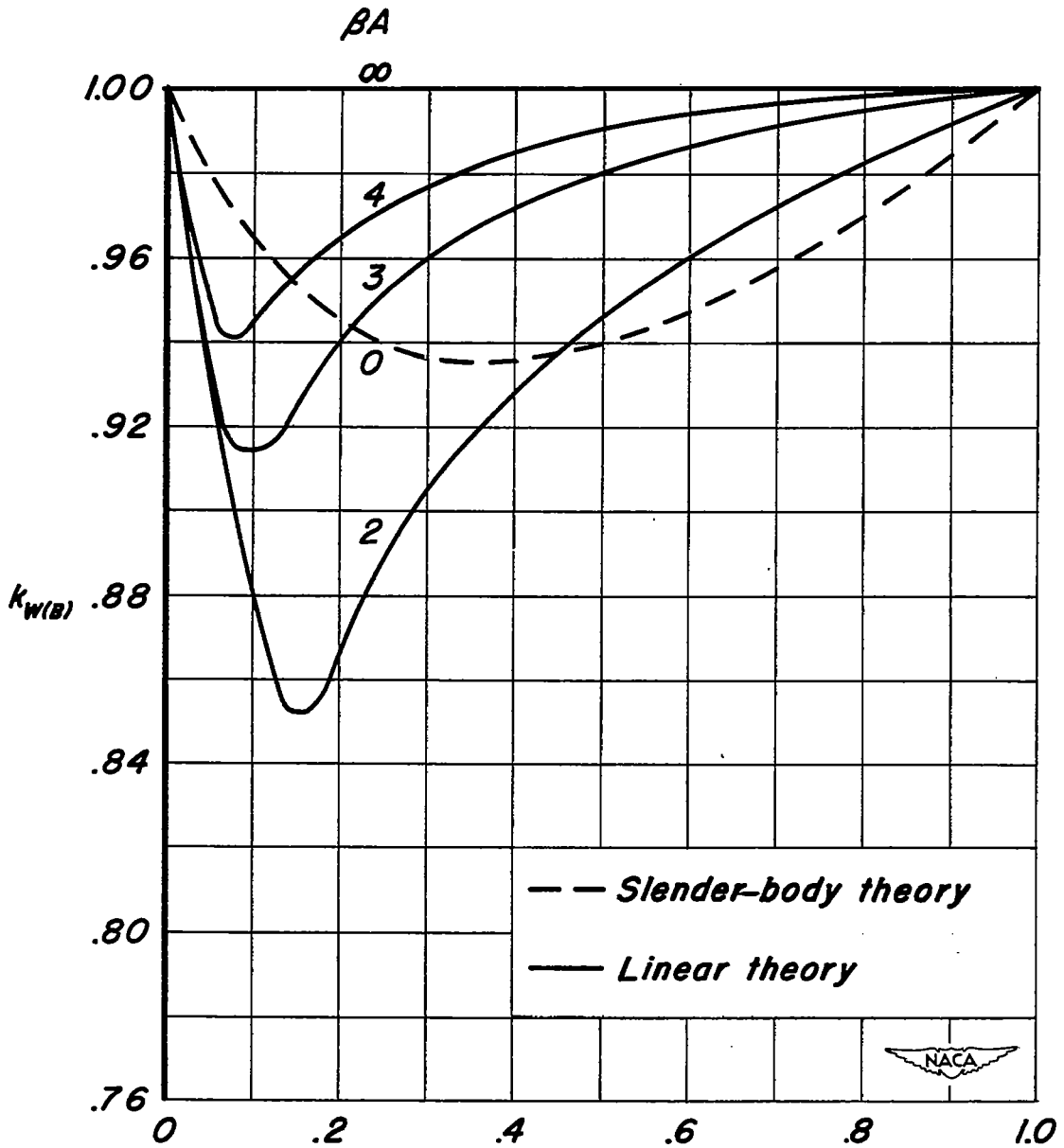

Figure 3.–Values of $k_{W(B)}$ for rectangular wing and body combinations.

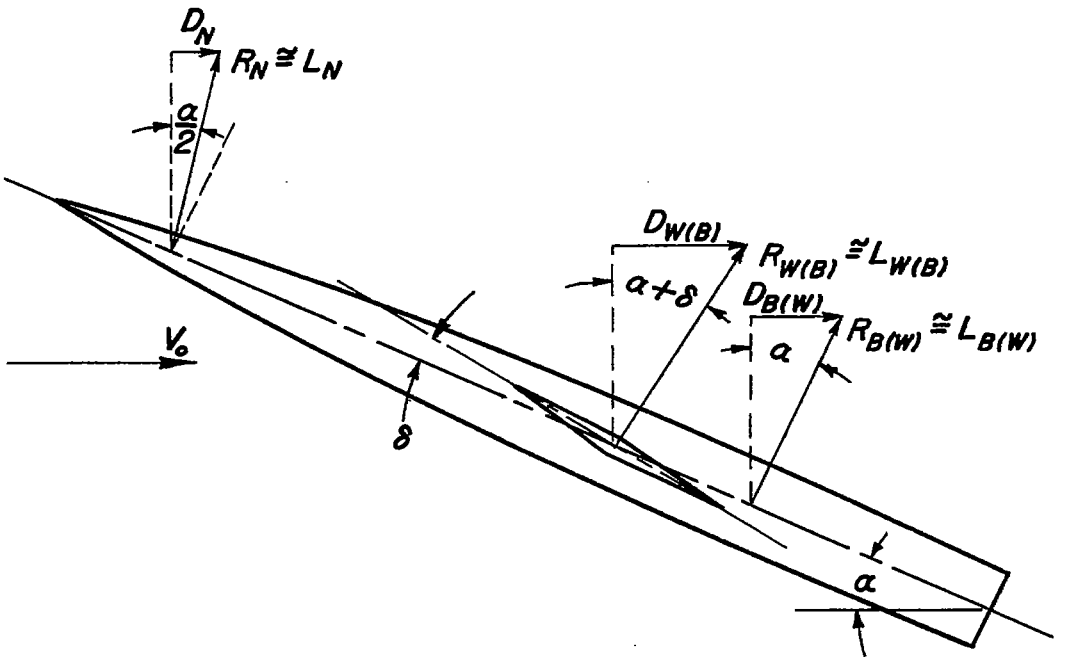

Figure 4.—Assumed inclination of resultant forces on components of wing-body combination.

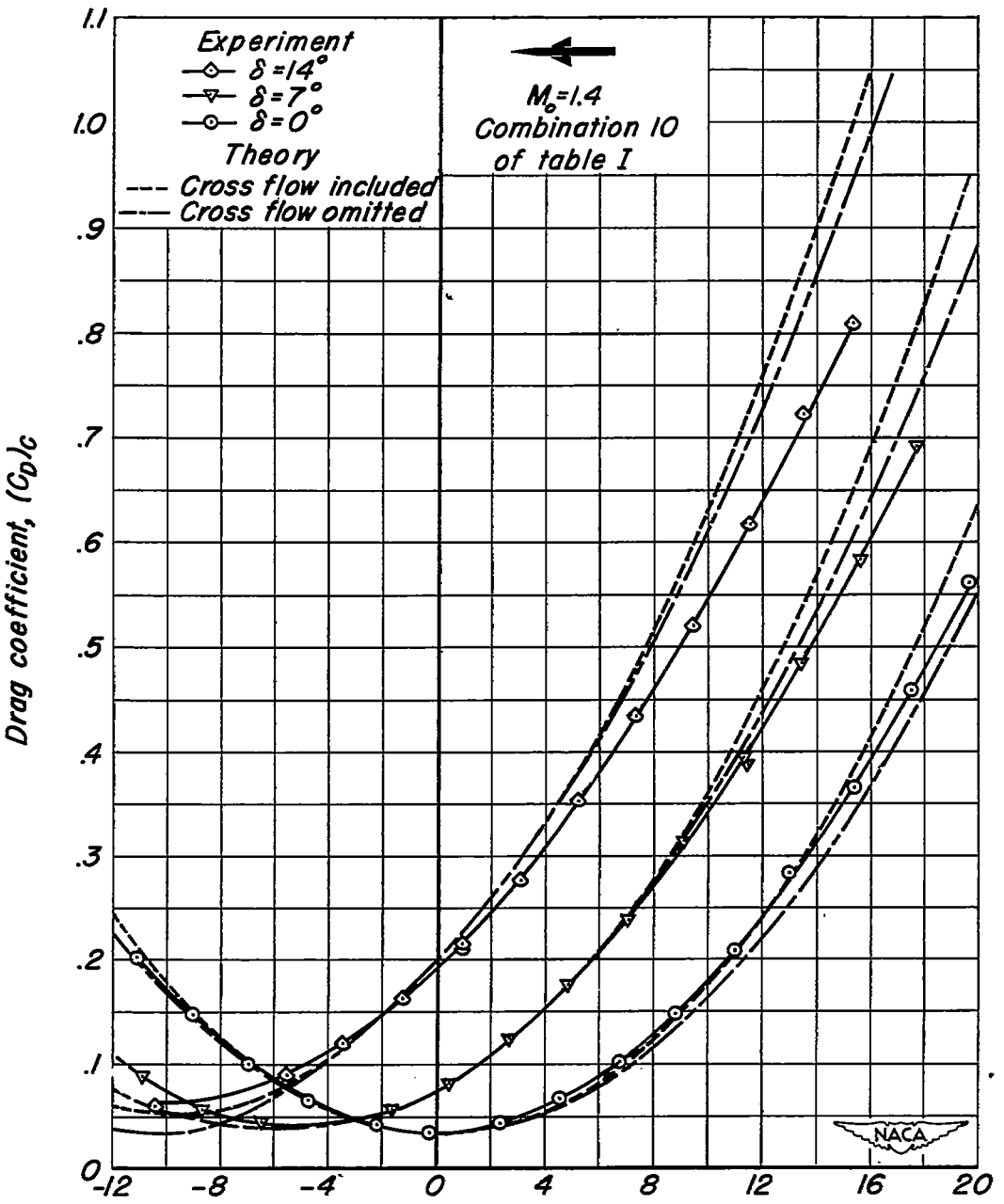

Figure 5.– Typical drag curves for a wing-body combination varying with angle of attack and having constant values of δ.

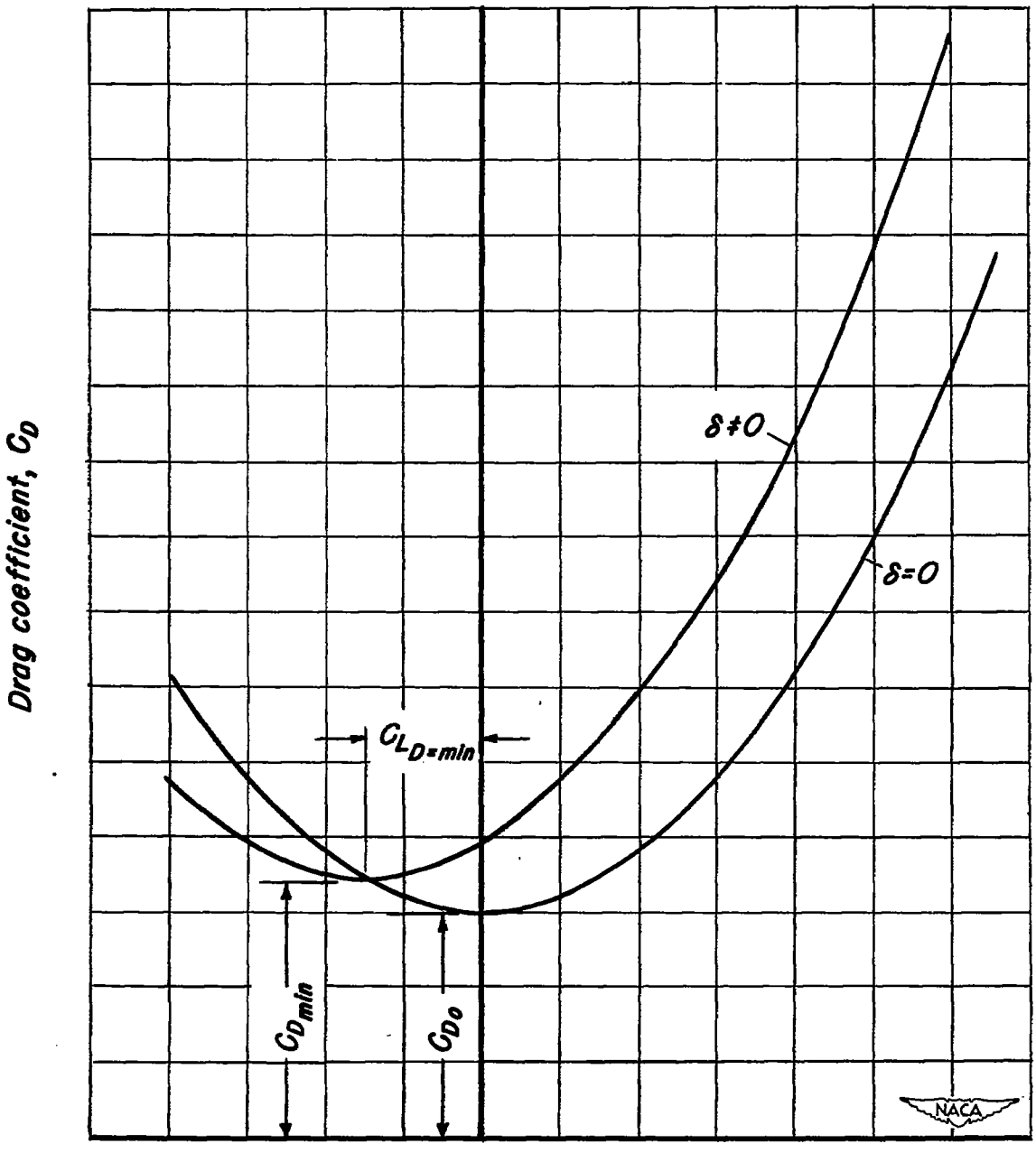

Figure 6.—Drag curves illustrating definition of terms.

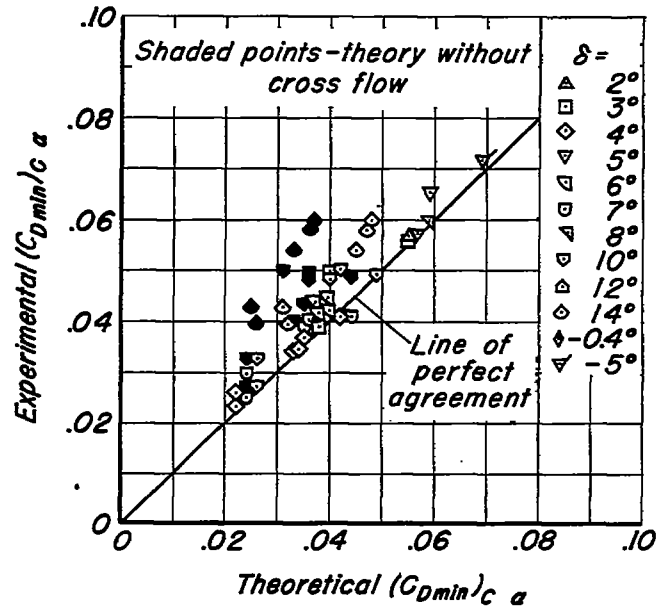

(a) Combination, α varying, δ constant.

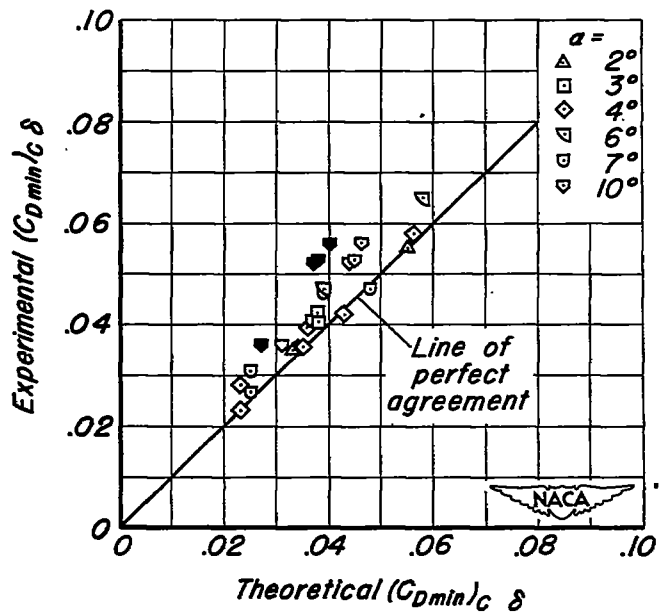

(b) Combination, δ varying, α constant.

Figure 7.- Comparison of experimental and theoretical minimum drag coefficients for wing-body combinations.

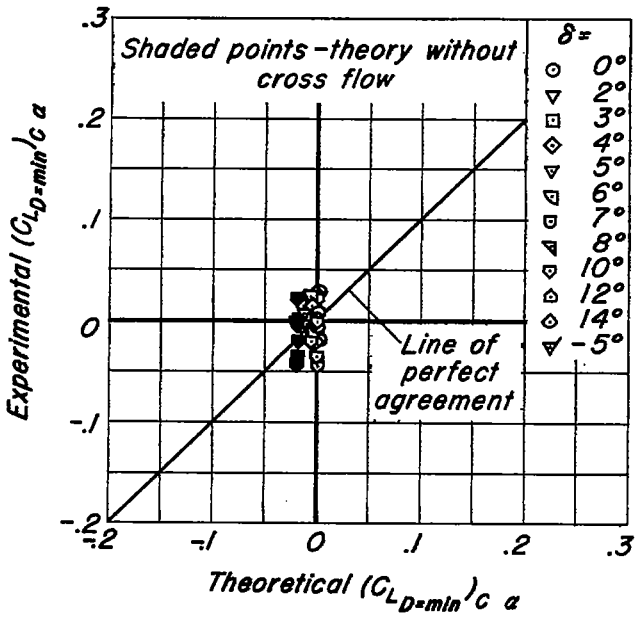

(a) Combination, α varying, δ constant.

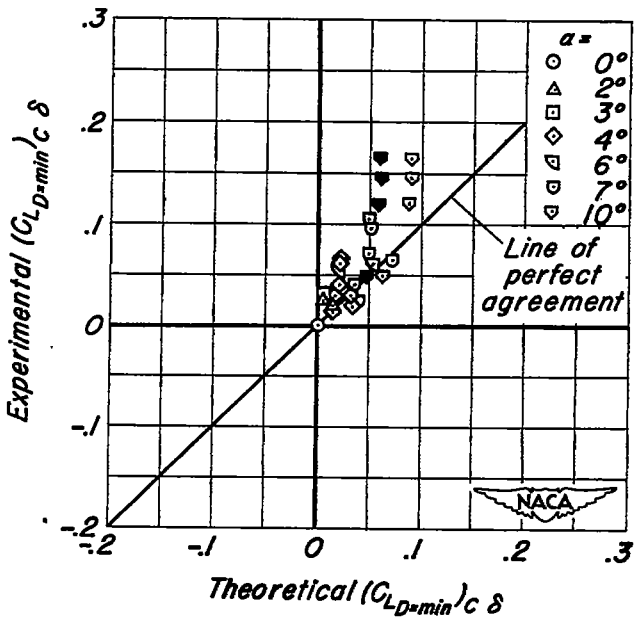

(b) Combination, δ varying, α constant.

Figure 8.- Comparison of experimental and theoretical lift coefficient for minimum drag.

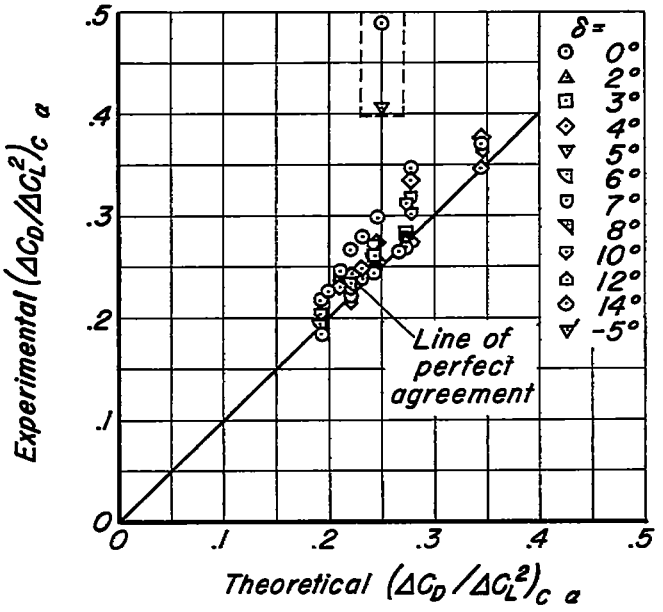

(a) Combination, α varying, δ constant.

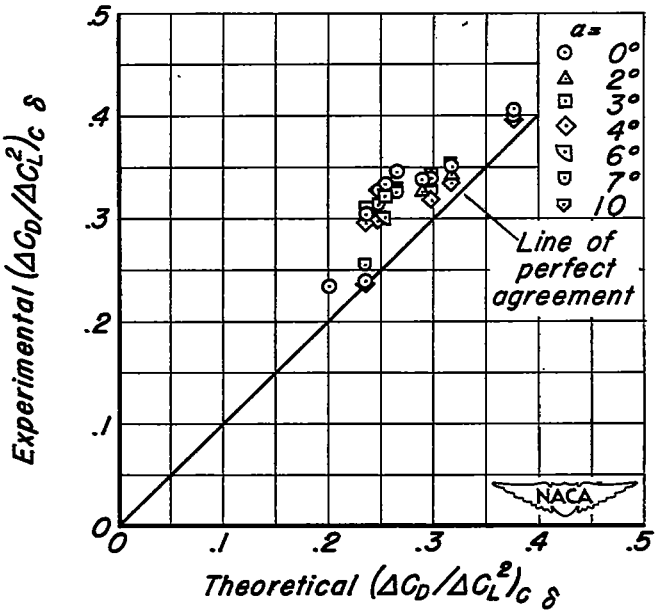

(b) Combination, δ varying, α constant.

Figure 9.- Comparison of experimental and theoretical drag-rise factors.

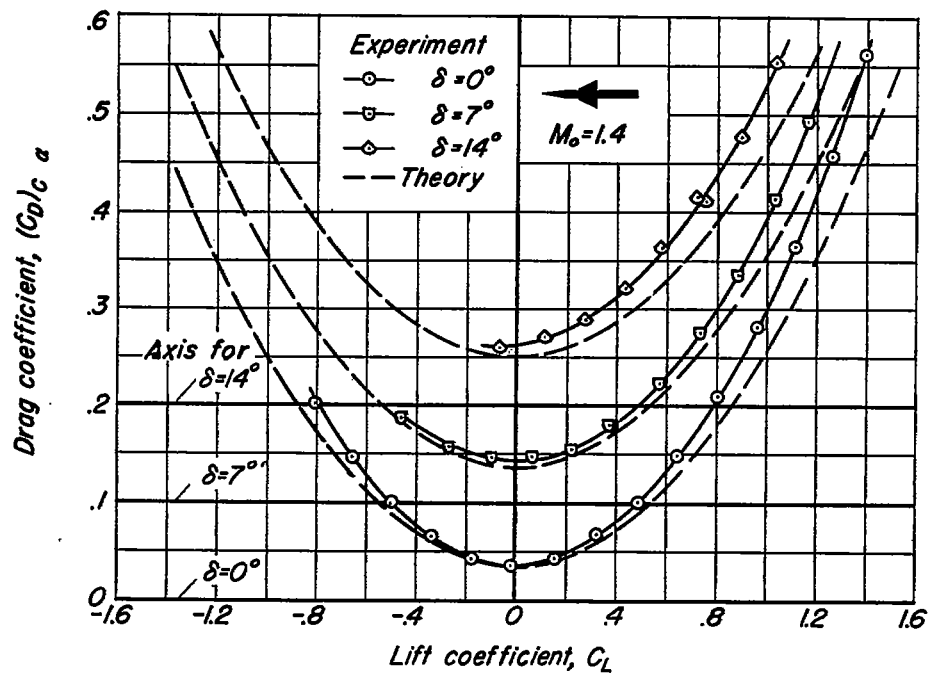

(a) Combination, α varying, δ constant.

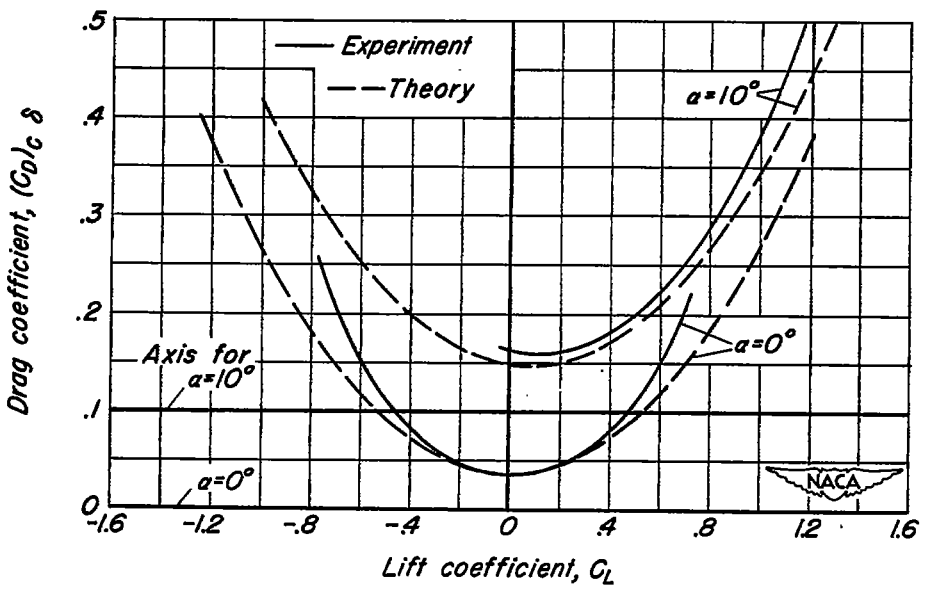

(b) Combination, δ varying, α constant.

Figure 10.- Typical drag curves for wing-body combination corresponding to combination 10 of table I.

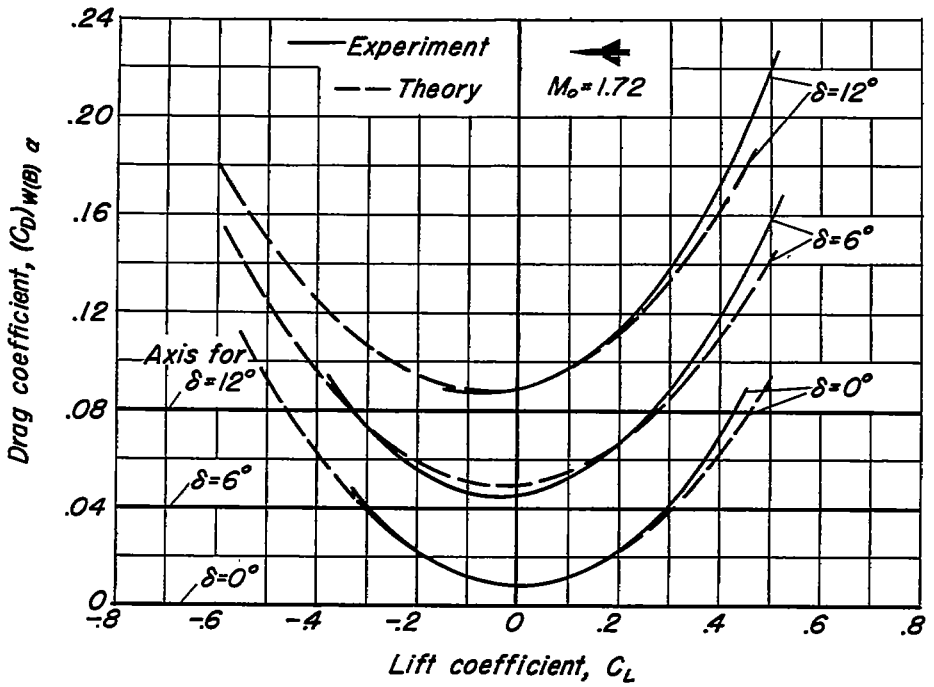

(a) Wing in presence of body, α varying, δ constant.

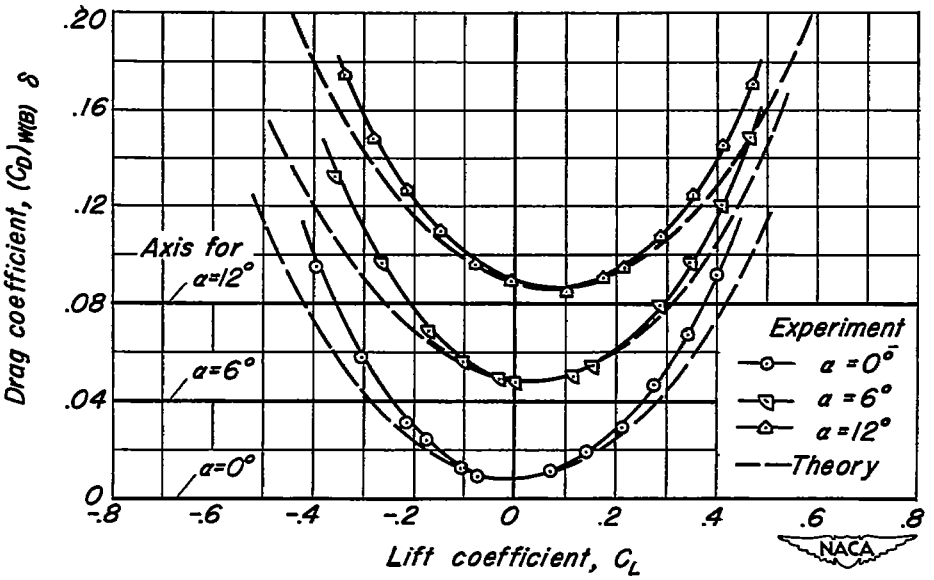

(b) Wing in presence of body, δ varying, α constant.

Figure 11.- Drag curves for wing in presence of body corresponding to combination 17 of table I.

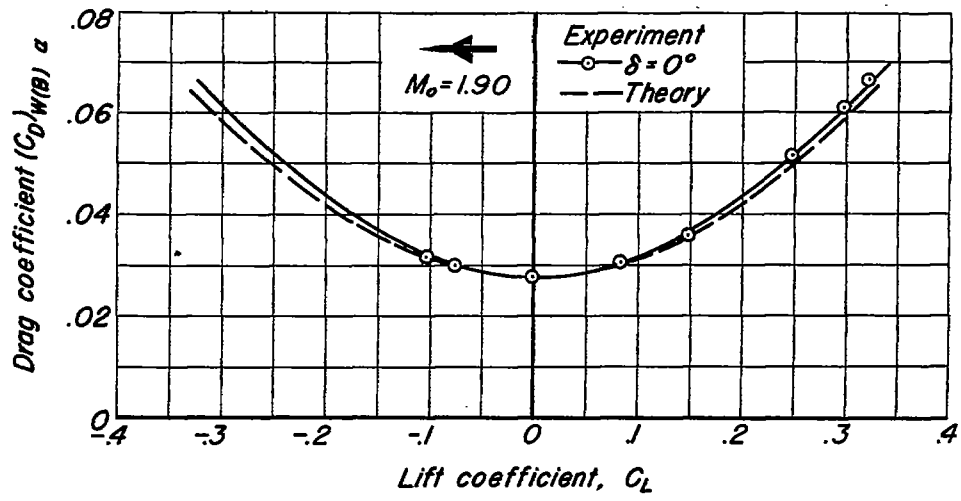

(a) Wing in presence of body, α varying, δ constant.

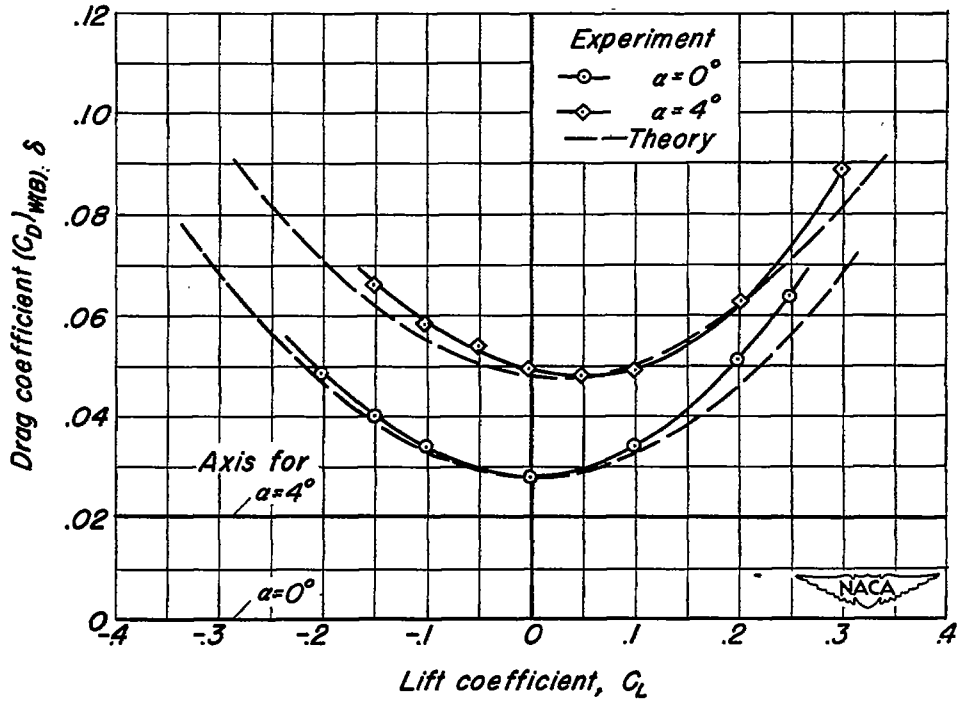

(b) Wing in presence of body, δ varying, α constant.

Figure 12.- Drag curves for wing in presence of body corresponding to combination 18 of table I.

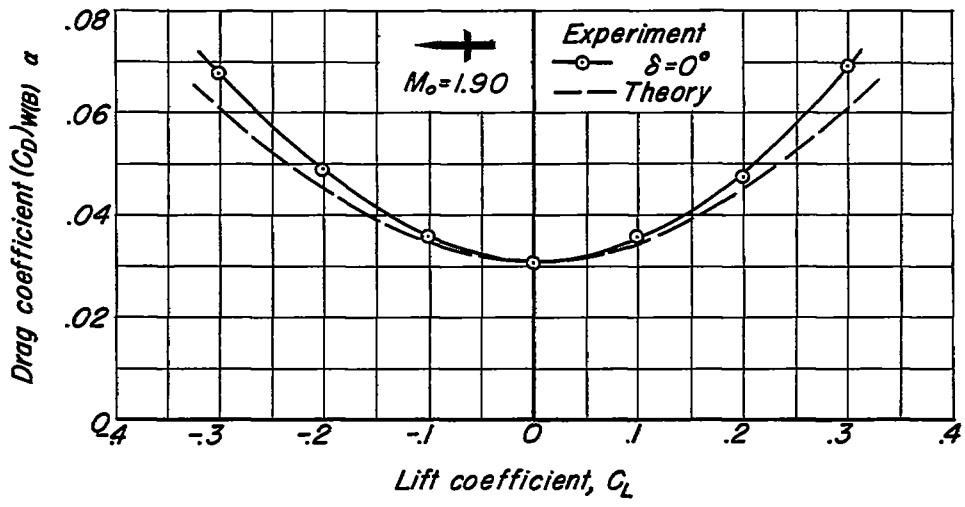

(a) Wing in presence of body, α varying, δ constant.

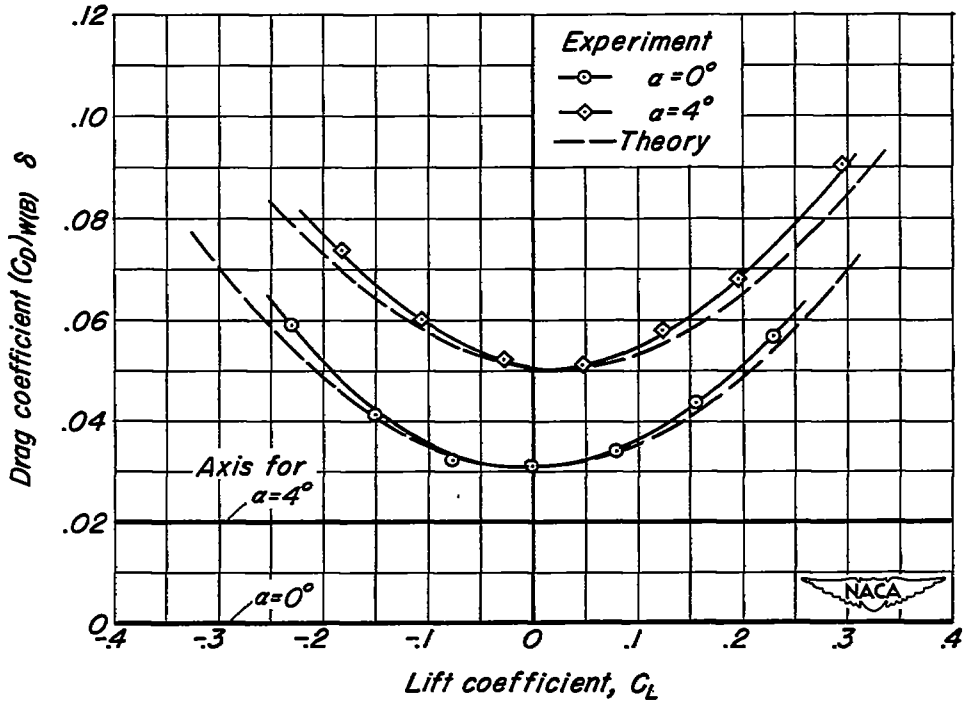

(b) Wing in presence of body, δ varying, α constant.

Figure 13.–Drag curves for wing in presence of body corresponding to combination 19 of table I.

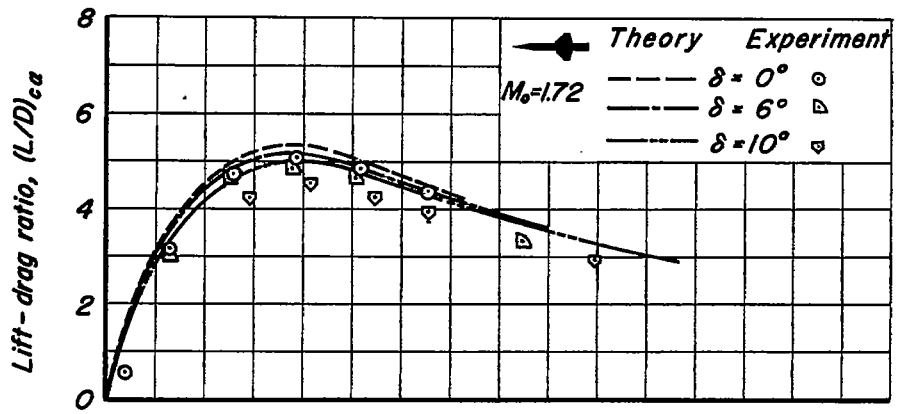

(a) Combination 1 of table I.

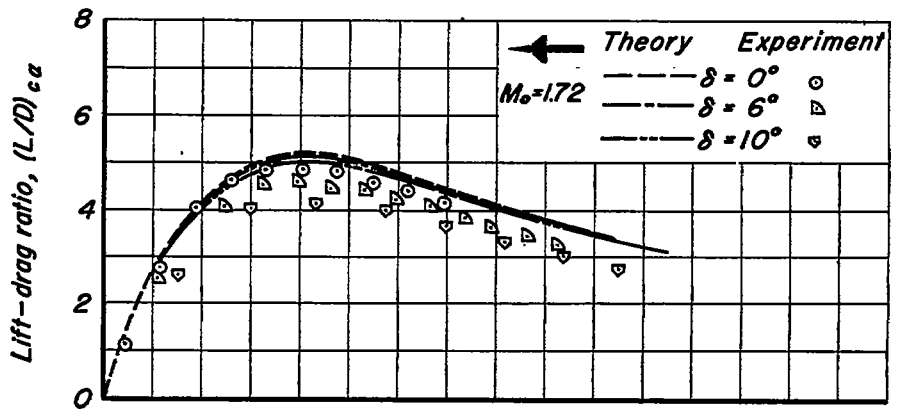

(b) Combination 2 of table I.

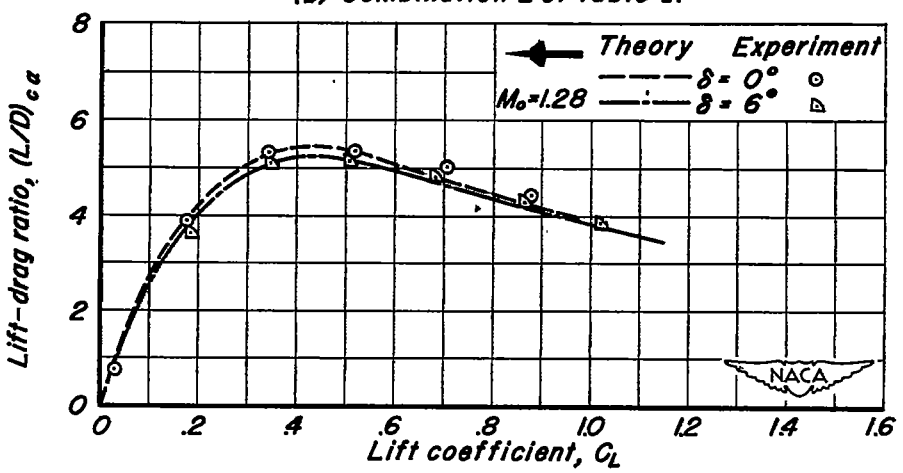

(c) Combination 3 of table I.

Figure 14.- Lift-drag ratios for constant values of wing deflection for the wing-body combinations of table I.

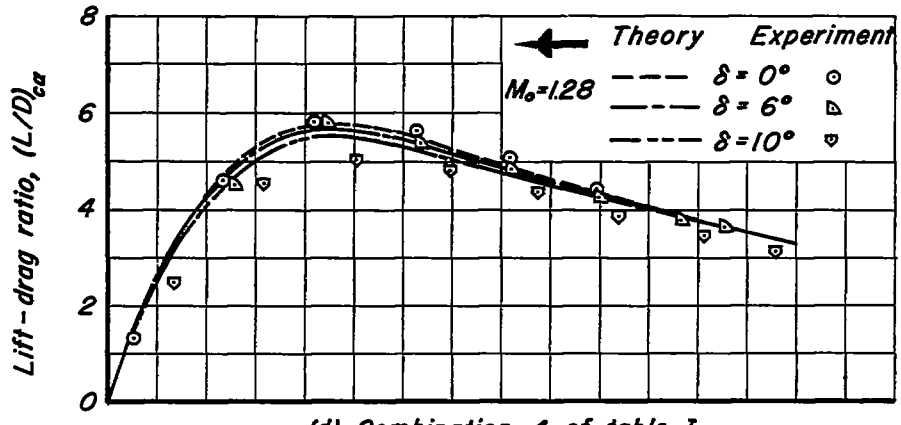

(d) Combination 4 of table I.

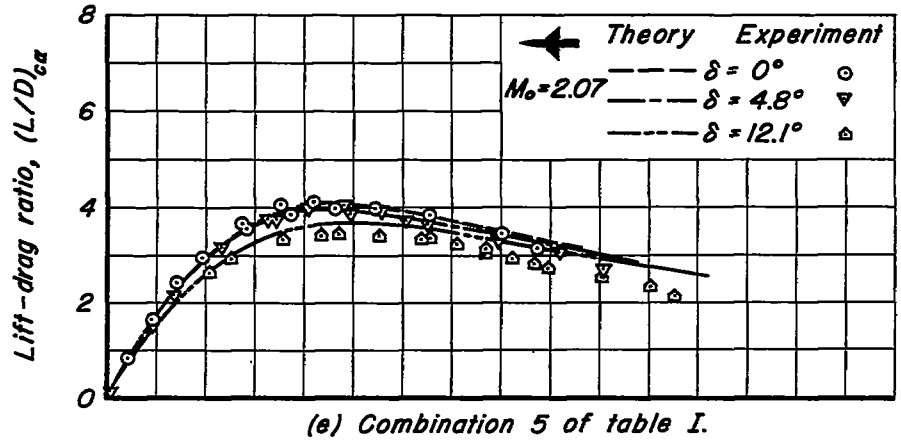

(e) Combination 5 of table I.

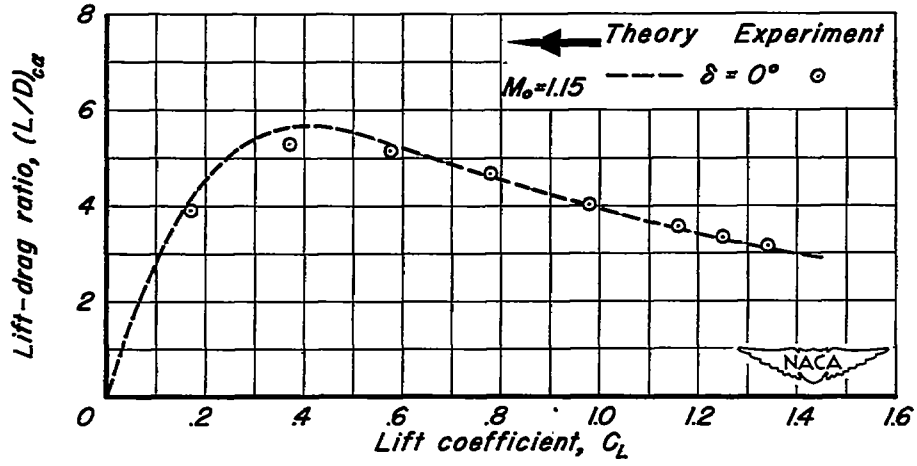

(f) Combination 7 of table I.

Figure 14.- Continued.

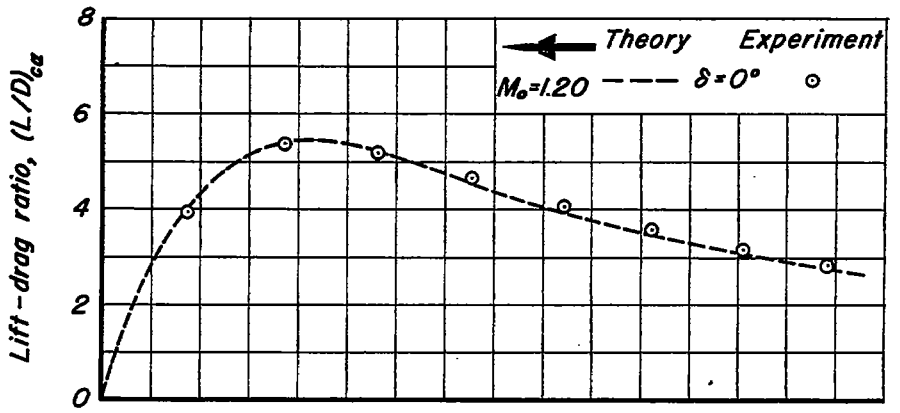

(g) Combination 8 of table I.

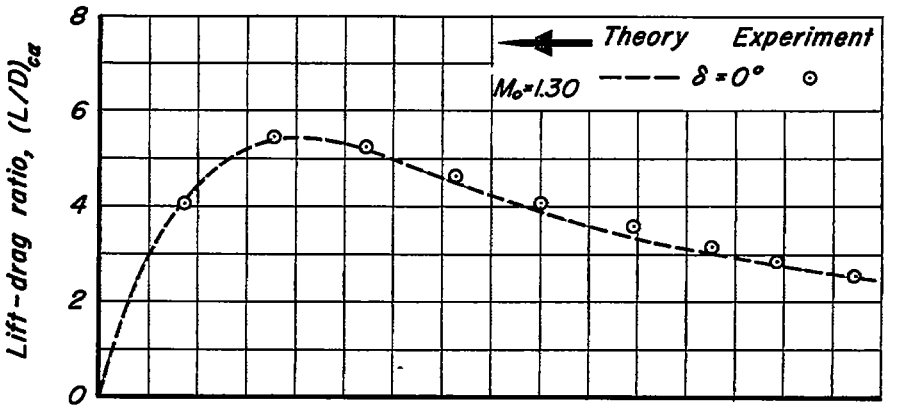

(h) Combination 9 of table I.

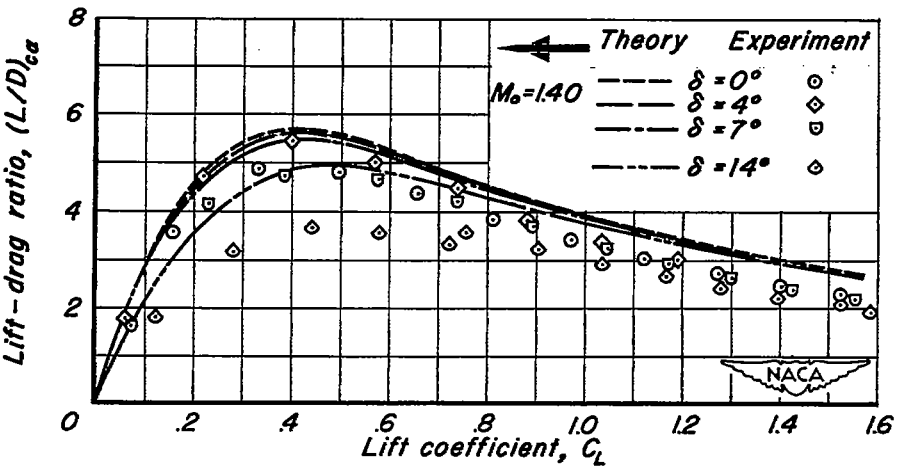

(i) Combination 10 of table I.

Figure 14.- Continued.

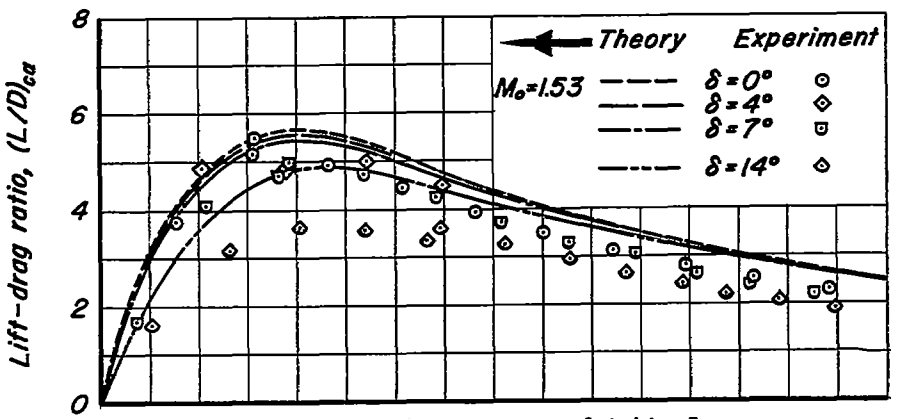

(j) Combination 11 of table I.

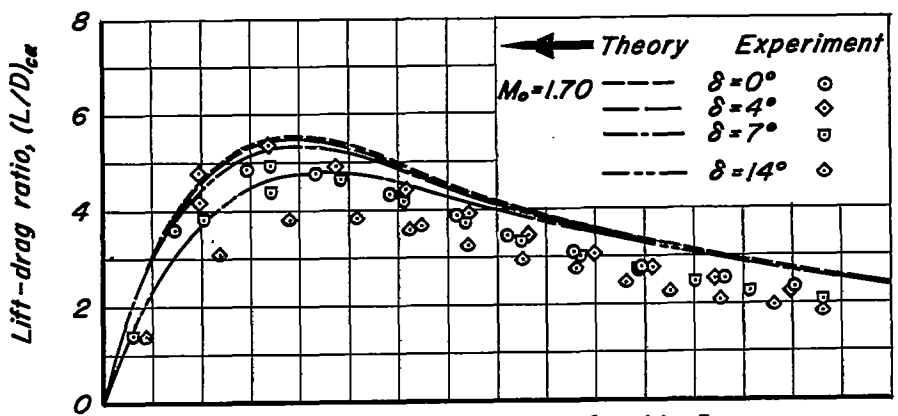

(k) Combination 12 of table I.

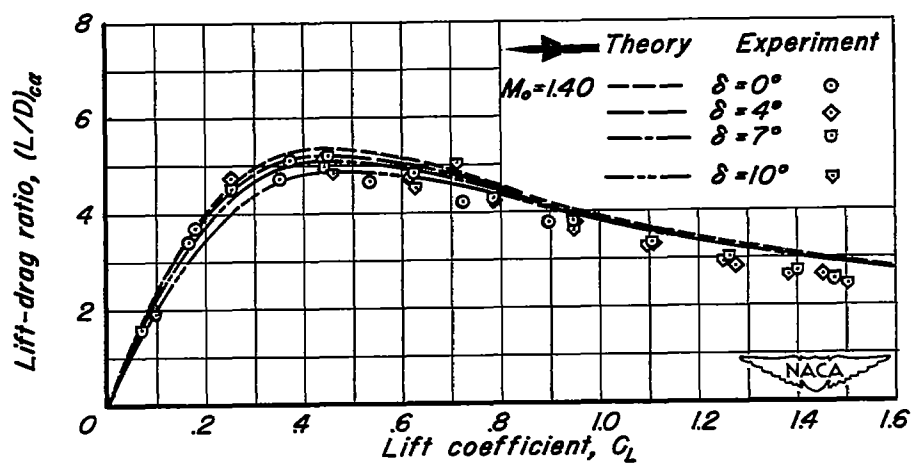

(l) Combination 13 of table I.

Figure 14.- Continued.

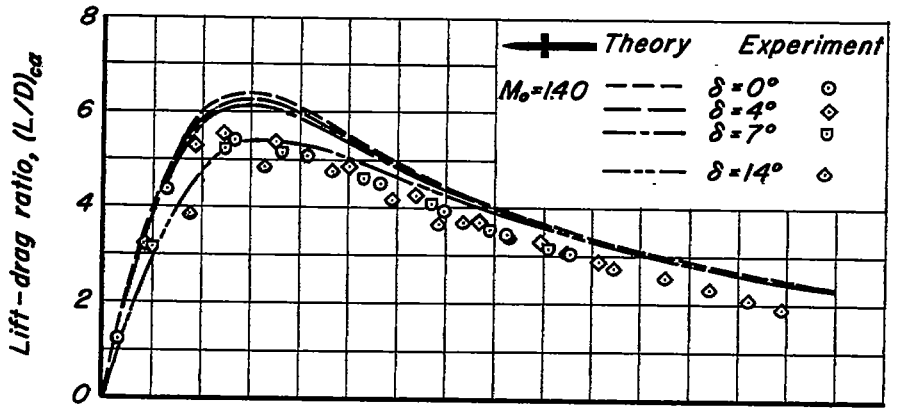

(m) Combination 14 of table I.

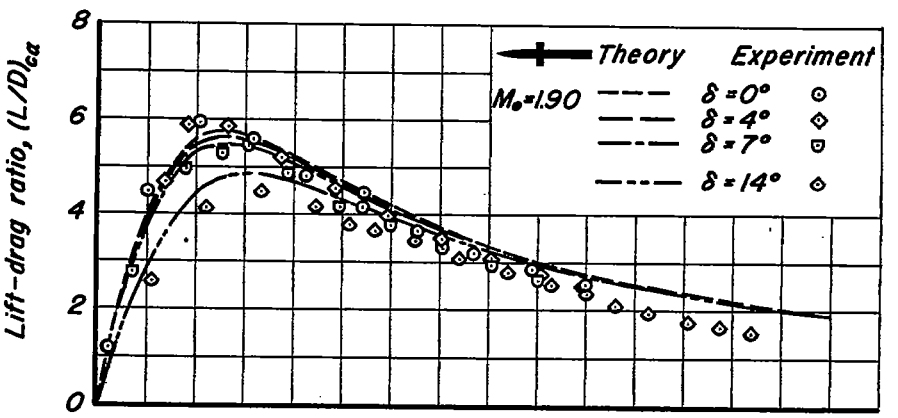

(n) Combination 15 of table I.

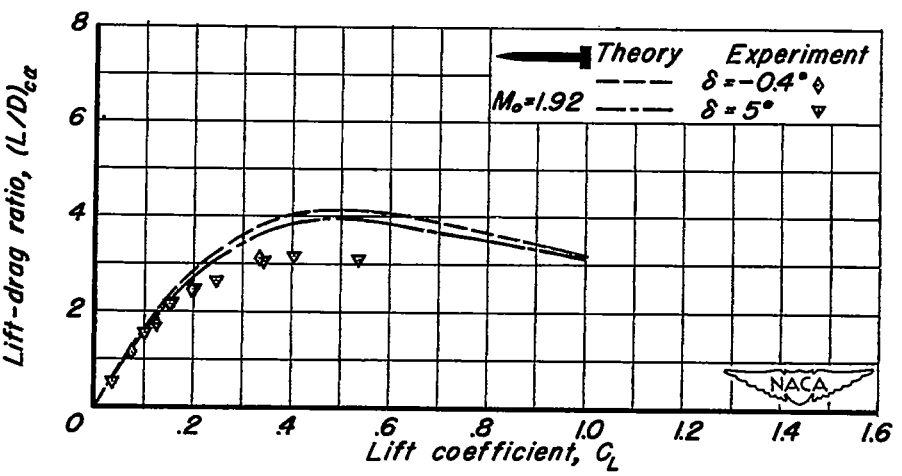

(o) Combination 16 of table I.

Figure 14. – Continued.

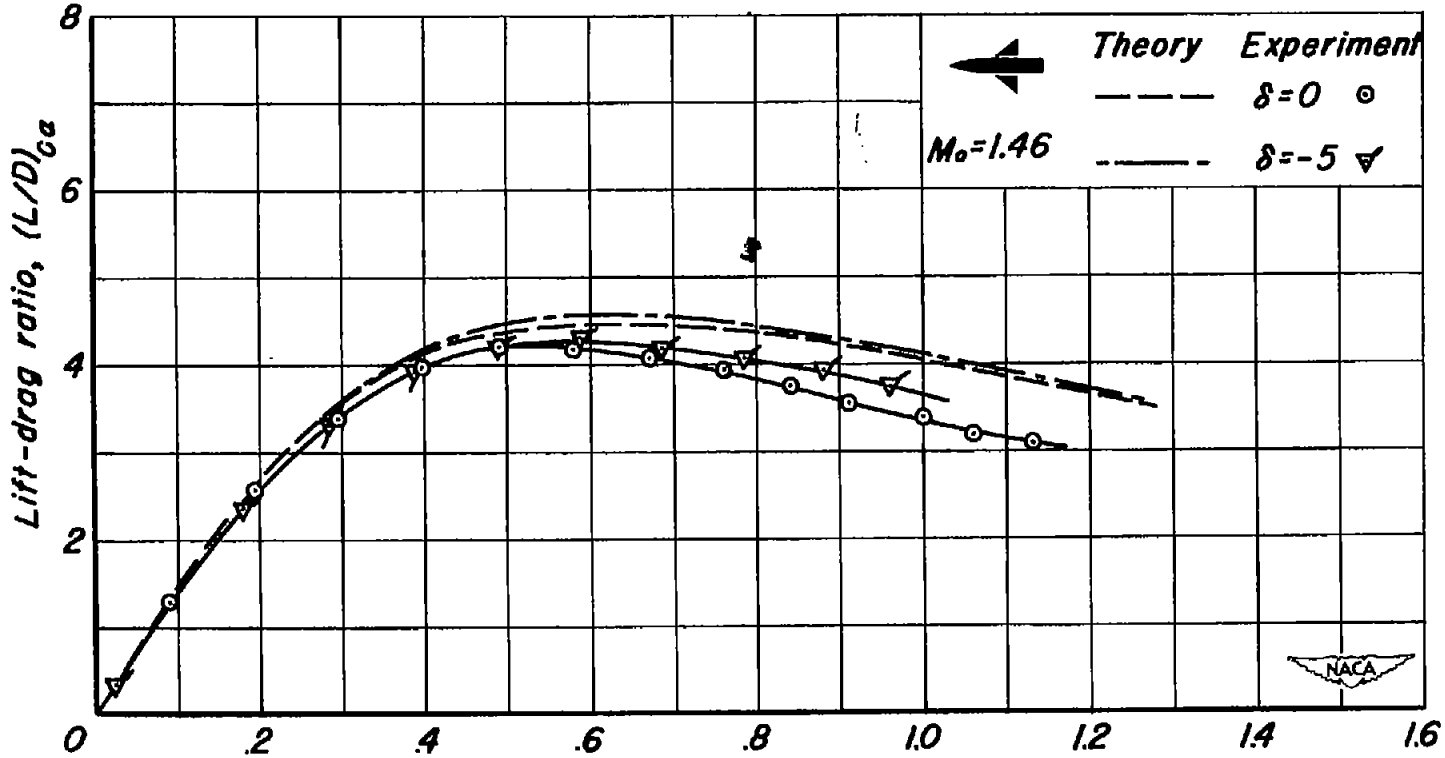

(p) Combination 6 of table I.

Figure 14.- Concluded.

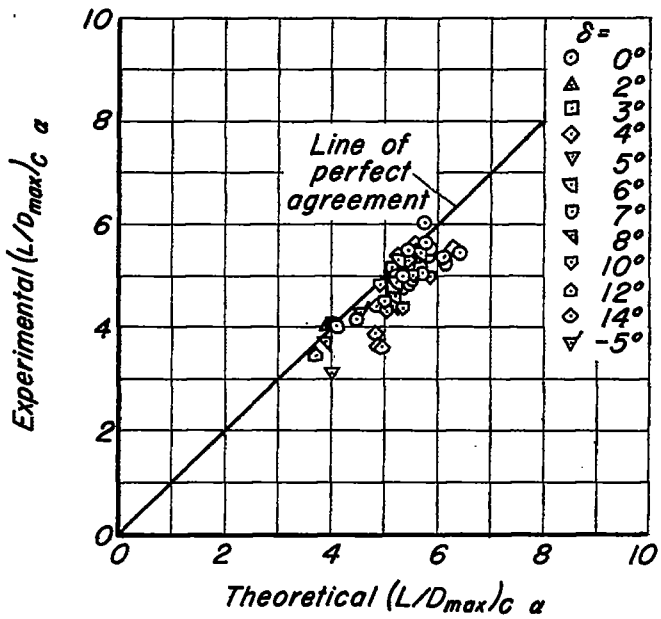

(a) Combination, α varying, δ constant.

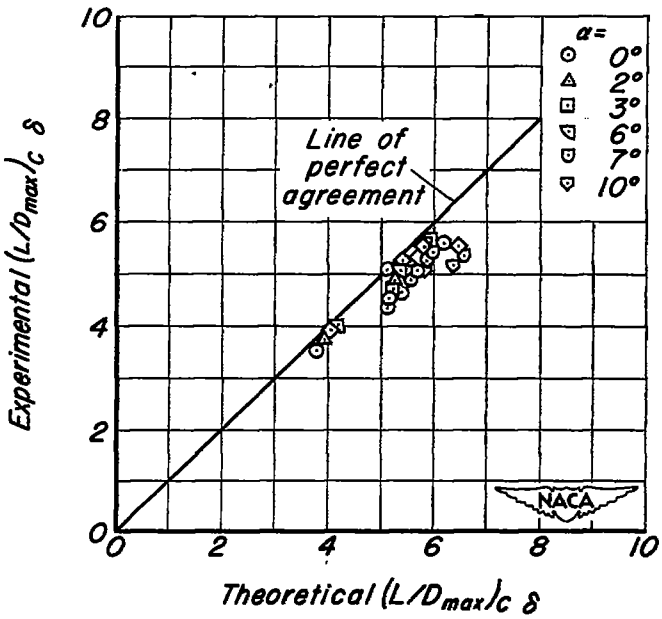

(b) Combination, δ varying, α constant.

Figure 15.–Comparison of experimental and theoretical maximum lift-drag ratios.

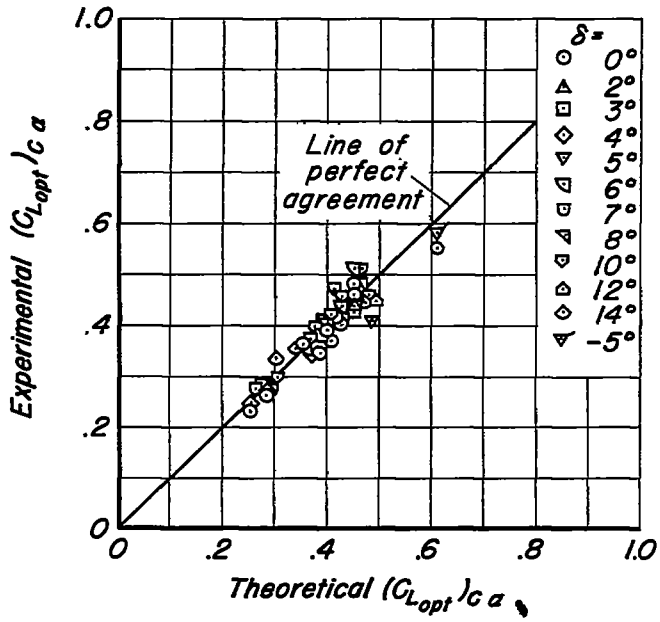

(a) Combination, α varying, δ constant.

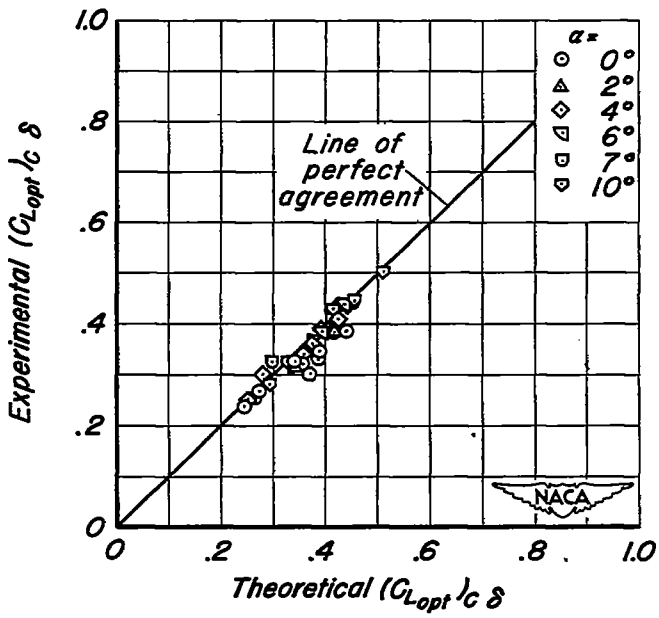

(b) Combination, δ varying, α constant.

Figure 16.- Comparison of experimental and theoretical lift coefficients for maximum lift-drag ratios.

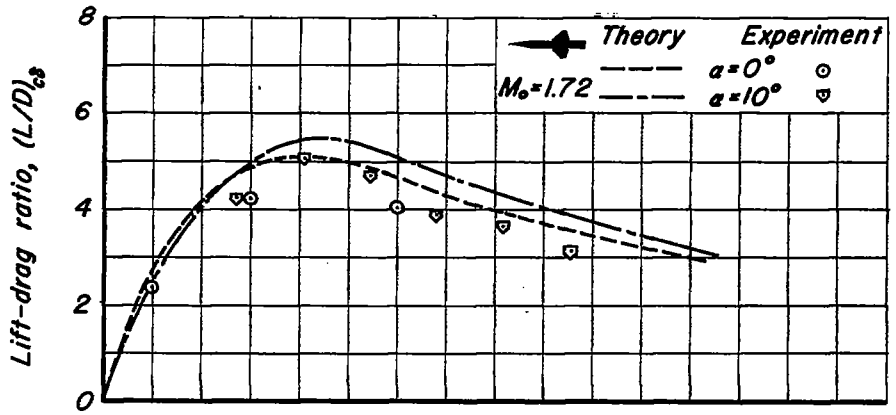

(a) Combination 2 of table I.

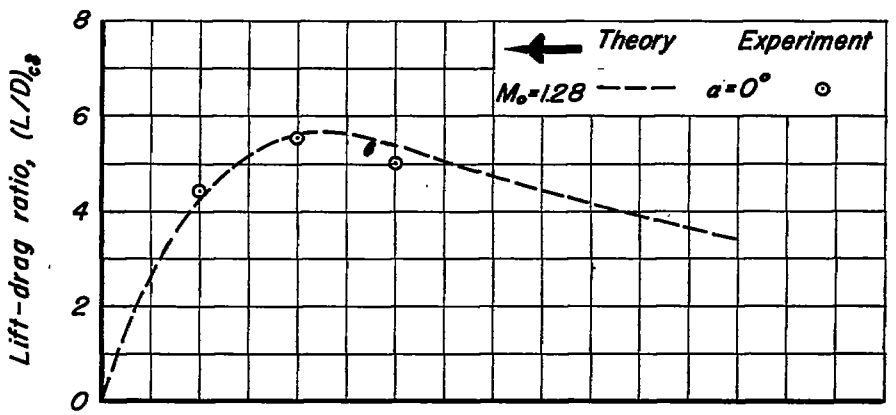

(b) Combination 4 of table I.

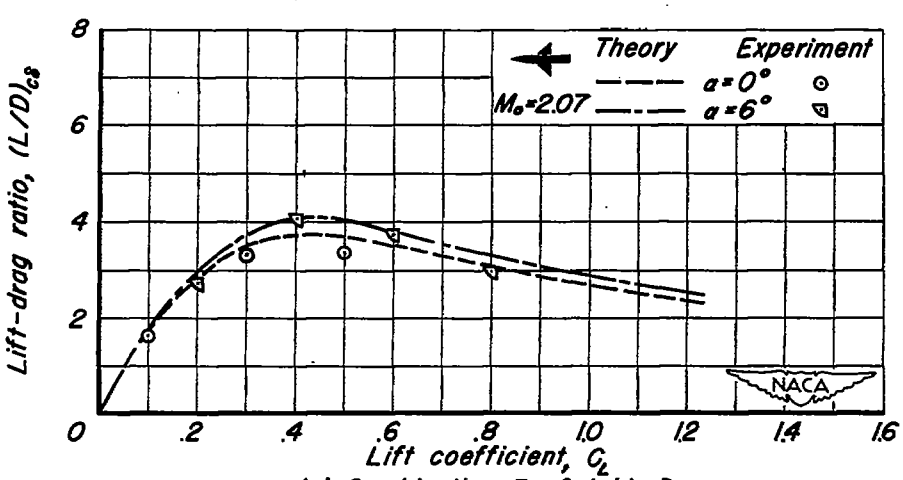

(c) Combination 5 of table I.

Figure 17.- Lift-drag ratios for constant values of angle of attack for the the wing-body combinations of table I.

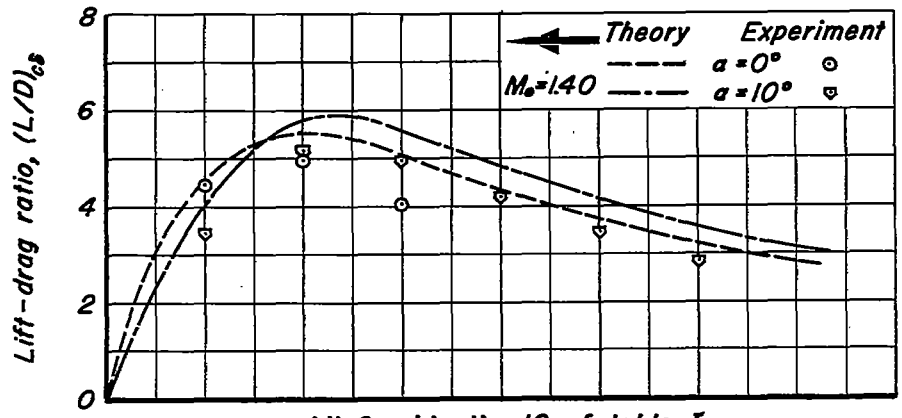

(d) Combination 10 of table I.

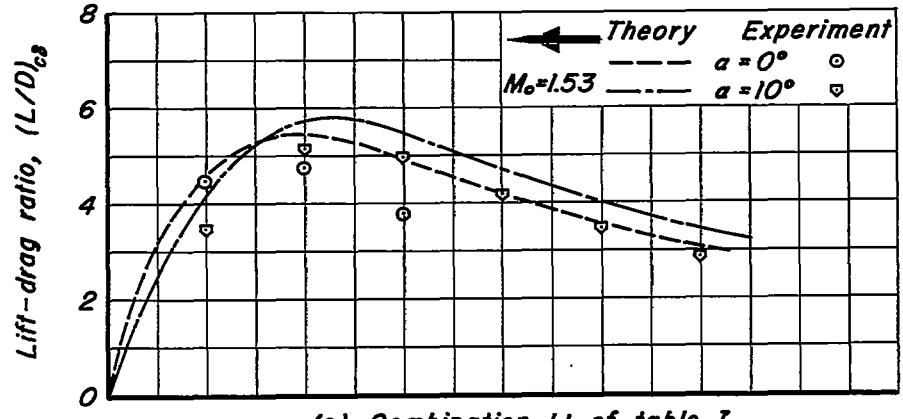

(e) Combination 11 of table I.

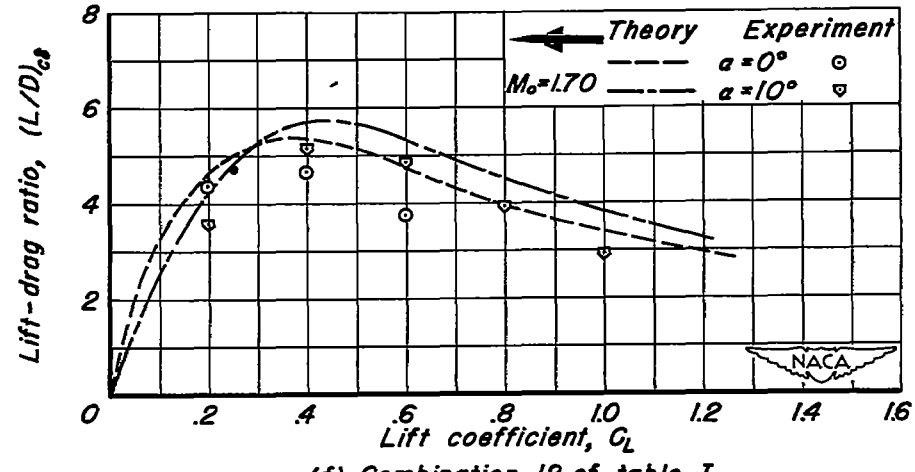

(f) Combination 12 of table I.

Figure 17.- Continued.

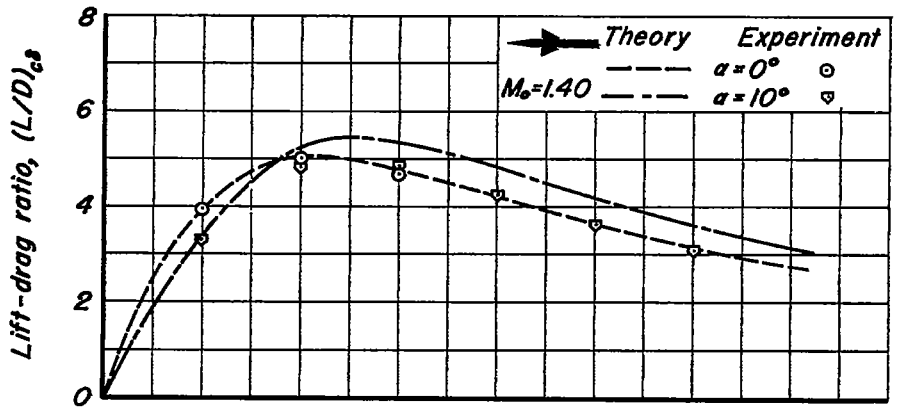

(g) Combination 13 of table I.

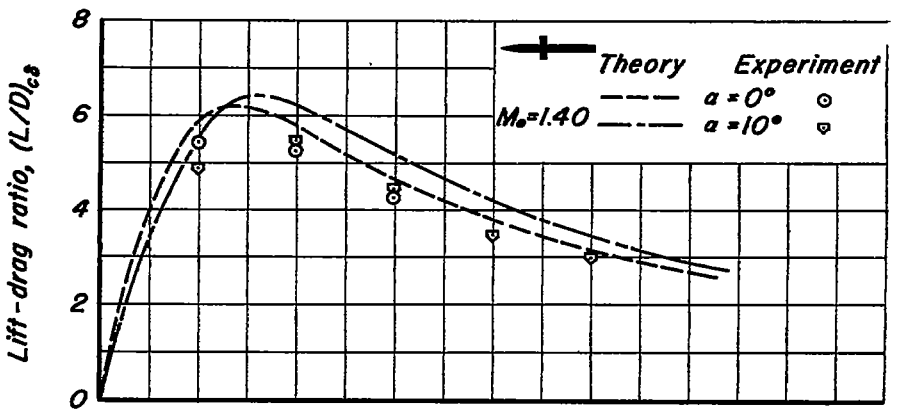

(h) Combination 14 of table I.

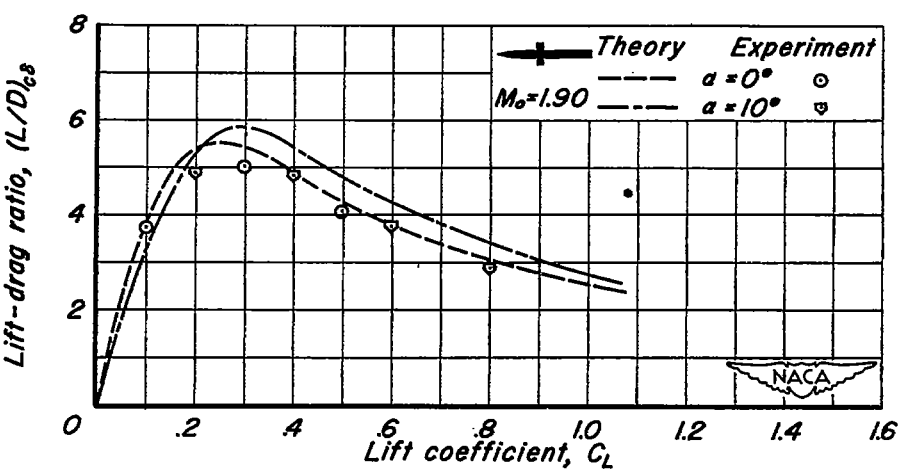

(i) Combination 15 of table I.

Figure 17. – Concluded.